LBL-2786
c.8

# LATTICE DEFECTS IN SPINELS

Omer Oscar Van der Biest
(Ph.D. thesis)

July, 1974

Prepared for the U. S. Atomic Energy Commission
under Contract W-7405-ENG-48

TWO-WEEK LOAN COPY

*This is a Library Circulating Copy which may be borrowed for two weeks. For a personal retention copy, call Tech. Info. Division, Ext. 5545*

LAWRENCE BERKELEY LABORATORY
UNIVERSITY OF CALIFORNIA
BERKELEY

LBL-2786
c.8

## DISCLAIMER

This document was prepared as an account of work sponsored by the United States Government. While this document is believed to contain correct information, neither the United States Government nor any agency thereof, nor the Regents of the University of California, nor any of their employees, makes any warranty, express or implied, or assumes any legal responsibility for the accuracy, completeness, or usefulness of any information, apparatus, product, or process disclosed, or represents that its use would not infringe privately owned rights. Reference herein to any specific commercial product, process, or service by its trade name, trademark, manufacturer, or otherwise, does not necessarily constitute or imply its endorsement, recommendation, or favoring by the United States Government or any agency thereof, or the Regents of the University of California. The views and opinions of authors expressed herein do not necessarily state or reflect those of the United States Government or any agency thereof or the Regents of the University of California.

# LATTICE DEFECTS IN SPINELS

## Contents

Abstract . . . . . v

1. Introduction . . . . . 1

2. The Structure and Properties of Lithium Ferrite . . . . . 4

3. Experimental . . . . . 7

4. Cation Stacking Faults in Lithium Ferrite Spinel . . . . . 9

4.1. Introduction . . . . . 9

4.2. Results . . . . . 9

4.2.1. Electron Microscopy--Disordered State . . . 9

4.2.2. Crystallographic Study of Cation Faults in Spinel . . . . . 13

4.3. Summary of Facts . . . . . 20

4.4. Discussion . . . . . 20

5. Domains in Ordered Lithium Ferrite-Enantiomorphism . . . . 23

5.1. Introduction . . . . . 23

5.2. Structural Information . . . . . 24

5.3. Contrast in the Electron Microscope . . . . . 26

5.3.1. Contrast at Domain Boundaries . . . . . 26

5.3.2. Contrast Between Domains . . . . . 29

5.4. Results . . . . . 30

5.4.1. Translation and Inversion Domains . . . . . 30

5.4.2. Stacking Faults in Ordered Lithium Ferrite . 32

5.5. Discussion . . . . . 35

6. General Discussion . . . . . 38

Acknowledgements . . . . . 41

References . . . . . 42

Tables . . . . . 46

Figure Captions . . . . . 53

Figures . . . . . 57

# LATTICE DEFECTS IN SPINELS

Omer Oscar Van der Biest

Inorganic Materials Research Division, Lawrence Berkeley Laboratory and Department of Materials Science and Engineering, College of Engineering; University of California, Berkeley, Calfironia

## ABSTRACT

A theoretical and experimental study has been made of some lattice defects in the spinel structure. Analyses have been done on $LiFe_5O_8$ single crystals using transmission electron microscopy.

From geometric and energetic arguments it has been shown that for a 1/4⟨110⟩ cation fault, the plane perpendicular to the displacement vector will have the lowest surface energy in a stoichiometric spinel. The influence of non-stoichiometry on the orientation of the fault plane is discussed.

Extended stacking faults have been found in flux grown lithium ferrite spinel single crystals, using high voltage electron microscopy. As predicted, the faults lie on {110} planes, and have a displacement vector of 1/4⟨110⟩ which is always perpendicular to the fault plane. The faults form three-fold junctions but can also be terminated by a dislocation with Burgers vector $\bar{b}$ = 1/4⟨110⟩.

At 750°C an order-disorder reaction takes place in lithium ferrite. The spacegroup symmetry is lowered from Fd3m (spinel structure) to $P4_132$ or $P4_332$. The ordered structure can exist in two enantiomorphous forms.

Simple electron microscopy techniques are described which allow one to detect the presence of two enantiomorphous forms of a structure

within an apparent single crystal. The first method consists of a characterization of the interface between the two enantiomorphs. In the second method advantage is taken of violations in Friedel's law which can occur in non-centrosymmetrical crystals. Methods which can be used to determine the absolute configuration of the structure in a part of the crystal are discussed. These techniques have been illustrated by an analysis of the domain structure in ordered $LiFe_5O_8$. Consistent results were obtained with both methods. The first method yields a more complete description of the domain structure.

Ordered lithium-ferrite contains boundaries of three different types (1) ordinary anti-phase boundaries, occurring within one enantiomorph, characterized by a displacement vector $\bar{R} = 1/2\langle 110\rangle$, (2) inversion boundaries characterized by an inversion operation, (3) boundaries described by an inversion and a translation. The contrast to be expected from each of these has been calculated. Each of these boundaries can be unambiguously identified by contrast experiments in the microscope. It has also been found that cation stacking faults can serve as a boundary between right and left-handed structures. In the ordered structure cation stacking faults can change character from $\{110\}$ $1/4\langle 110\rangle$ type to $\{110\}$ $1/4\langle \bar{1}12\rangle$ type.

# 1. INTRODUCTION

In today's technology, the performance of a product is often limited by the properties of the materials used. The realization of a new design is often held up or made impossible by the lack of the required materials. There is a continuous need for new and better materials. In industry, there is always the pressure to find cheaper substitutes. Modern engineering designs often require materials with a combination of properties which are not available in a single material. Ideally, one would have the ability to design a material with a particular application in mind, whereas now one has to adapt the design to existing materials.

Whatever "materials design" there has been, it has often been based on empirical rules acquired through experience and which have to be supplemented by an extensive and expensive testing program. It is the goal of the modern materials scientist to be able to design a material from first principles, that is from the appropriate theoretical model. In the area of alloy design and especially in steels, one is coming close to this goal. In ceramic materials, however, one still has a very long way to go. One reason for this is that the microstructure of existing ceramic materials has not been characterized in as much detail and with the same resolution as metallic materials. Specifically, much is still to be learned about the mechanisms of phase transformations in these ceramic materials, in particular, about the crystallographic aspects, the early stages of a transformation and the role of crystal defects.

Line and planar defects have been shown to be very important in our understanding of phase transformations and mechanical properties in metals. Accordingly, these crystalline defects have received considerable attention in the scientific literature. By comparison, research on crystalline defects in ceramic compounds and minerals is in its infancy. Although the importance of these defects in the study of mechanical properties[1] and magnetic properties[2] has been demonstrated, the bulk of published work has been done on simple ionic structures, e.g., MgO[3] and on layer structures.[4] Recently, publications have appeared dealing with transition metal carbides.[5]

The electron microscope is the main experimental tool available for the study of crystalline defects. Recent advances in thinning techniques and the increased penetration power available through high voltage microscopes has made virtually every material accessable, and as a result, there is now an increase in research in ceramics and minerals.

Even if one limits oneself to ceramic materials, which find practical use, one finds a great diversity of crystal structures. Dislocation reactions and planar defects which have been found in one crystal structure can generally not be expected to occur in other structures as their occurrence depends in large part on the details of the structure. Hence, these have to be examined theoretically and experimentally in each structure.

In this work, a study is made of defects in the spinel structure. A great many compounds of practical significance take this structure. For instance, there are the refractory oxides $MgAl_2O_4$ and $(MgFe)(AlCr)_2O_4$. The ferrites $MFe_2O_4$, where M can be one of many metallic cations, are

important because of their ferrimagnetic properties. A theoretical study is made here of the cation stacking faults in the general spinel structure. The predictions are compared with the experimental observations on lithium ferrite ($Li_{0.5}Fe_{2.5}O_4$). This compound also exhibits an order-disorder reaction.[6] The resulting domain structure can be predicted from structural considerations and has been verified experimentally. $Li_{0.5}Fe_{2.5}O_4$ can be considered the prototype of a series of lithium containing spinels which form the same superstructure at lower temperatures: e.g., there are $LiM_{0.5}Ti_{1.5}O_4$, with M = Mg, Mn, Co, Zn, Cd; $LiM_{0.5}Mn_{2.5}O_4$ with M = Mg, Zn; $LiMGe_{1.5}O_4$ with M = Ni, Co, Zn[7] and $LiAl_5O_8$.[6]

## 2. THE STRUCTURE AND PROPERTIES OF LITHIUM FERRITE

Lithium ferrite is a ferrimagnetic material with some interesting technological properties which have been compiled by Von Aulock.[8] In polycrystalline form and with proper processing a rectangular hysteresis loop can be obtained.[9-14] This makes lithium ferrite a material useful for switching devices. Moreover, it has a Curie temperature around 630°C,[8] which is much higher than any other commonly used ferrite. This means that around room temperature its magnetic properties are less sensitive to temperature variations. Some of the properties which stand in the way of a widespread use of lithium ferrite for microwave applications are its low dc resistivity and its high dielectric loss. These properties have been related to lithium and oxygen loss during processing.[15-17]

Lithium ferrite ($Li_{0.5}Fe_{2.5}O_4$) has an inverse spinel structure (general formula $AB_2O_4$) with $Fe^{3+}$ on tetrahedrally coordinated sites (A-sites) and a 3:1 mixture of $Fe^{3+}$ and $Li^+$ on the octahedral sites (B-sites). Below 750°C $Fe^{3+}$ and $Li^+$ on the octahedral sites order. The ordered structure will be described in detail in Section 5.2.

Some important properties of the material show a marked dependence on the degree of order. Folen[18] and Schnitzler, et al.[19] showed that the magneto-crystalline anisotropy constants for the ordered and disordered state are widely different especially at low temperatures. Denton and Spencer[20] determined the ferrimagnetic resonance linewidth as a function of temperature for different states of order in the crystal. Another important property which shows a very strong dependency on the degree of order is the dc electrical resistivity. According to Kato[21]

the room temperature resistivity of disordered polycrystalline lithium-ferrite increases upon ordering by a factor of about $5\times10^4$. Kato[21] studied the order-disorder reaction using electrical resistivity measurements, dilatometry and differential thermal analysis. According to his results the transition temperature did not vary very much (±1°C) with deviations from stoichiometry to the lithium rich and iron rich side. The question can be raised here if the specimens used were truly homogeneous even though no second phases were detected by X-ray diffraction. A small thermal effect was found around the transition temperature but this observation could not be confirmed by Strickler and Roy.[24] Kato[22] also determined the long range order parameter as a function of temperature. A curve was obtained which came close to the one calculated by Gugenheim[23] for $Cu_3Au$. The order disorder transition is accompanied by a slight change in lattice parameter ($a_o \approx 8.33$A at room temperature and $\Delta a/a \approx 25.10^{-5}$ at the transition temperature[25]).

Above the critical temperature for long range order, a state of short-range order replaces the superstructure. Brunel and de Bergevin[26] measured the X-ray diffuse scattering due to short range order on quenched powder samples (temperatures 797°C and 893°C). A theory of X-ray diffuse scattering in $LiFe_5O_8$ was proposed by Yamada and Yoshimori.[27] The sites on which the ordering takes place can be divided up into tetrahedra, which in the ordered structure contain three iron and one lithium ion. It was proposed that in the short range ordered state the tetrahedra are still occupied by three iron and one lithium. Isodiffusion lines around reciprocal lattice points were calculated. After averaging these for a powder sample, good agreement was obtained with the experimental results.[26]

The physical picture emerging from this work is that the structure goes from long range order to short range order by randomisation of the iron and lithium ions on the tetrahedra.

Some electron microscopic observations on $LiFeO_2$ by Allpress[28] are also of interest here. Small precipitates of $Li_{0.5}Fe_{2.5}O_4$ were found in this material. Some of these precipitates in the ordered state exhibited internal boundaries along a crystallographic plane, which were interpreted as anti-phase boundaries. An electron metallographic study of the order disorder transition on bulk material has not yet appeared in the literature.

## 3. EXPERIMENTAL

Flux grown single crystals of $LiFe_5O_8$ were obtained from Airtron Litton Industries. Chemical analysis by flame photometry indicated that the crystals were slightly lithium deficient with an Fe/Li ratio of 5.43. In diffraction patterns, the as received crystals displayed all the superlattice reflections which were reported by Schieber.[29] A Buerger's precession camera was used to check the spacegroup symmetry of the structures involved.

Specimens for electron microscopy were prepared by two techniques, chemical polishing and ion bombardment. Chemical polishing was done by dipping a thin slice of the material in hot ortho-phosporic acid (250-300°C) and allowing it to dissolve until the specimen became transparant at the edges. The success of the method was found to depend on the orientation of the slice. Slices parallel with (111) often showed a high density of etch pits in the microscope. Etching along internal boundaries e.g., stacking faults or anti-phase boundaries was also a problem. Another disadvantage of this technique was that the sample had to be held at a rather high temperature for about 15 min. This could change the microstructure e.g., the state of order in our case. Apart from the etching along boundaries the foils produced by this method were quite satisfactory. Foils were also obtained using an ion bombardment technique[30] starting from standard thin sections (about 30μ thick).

Both methods of preparation cause the appearance of characteristic artefacts in the foil. The surface of chemically polished foils is especially prone to radiation damage in the microscope. The dislocation

loops, which form as a result, have been observed and analysed by De Jonghe and Thomas.[31] Foils, prepared by ion bombardment, usually exhibit some surface irregularity, which is disturbing only when the crystal is in a strongly diffracting condition. A theory to explain this surface topography has been put forward recently by Barber et al.[32] Foils prepared by this method did not exhibit the relatively large dislocation loops which are prominent in chemically polished foils. By preparing foils from the same specimen using the two methods of preparation, and comparing them, the artefacts introduced by either method could readily be distinguished from features, representative of the material. Thin areas damaged in the electron microscope could also be removed by ion bombardment after which the specimen was ready for examination again. All observations were made using a Hitachi 650KV microscope equipped with a double axis high angle tilt stage allowing a tilt of ±30° in either direction. This attachment allowed the study of a particular defect under widely different diffracting conditions and helped considerably in the identification of the defects. Tilting into required orientations was greatly facilitated by using the Kikuchi maps for silicon,[33] which resemble closely those for the spinel structure, allowing for differences in structure factor.

# 4. CATION STACKING FAULTS IN LITHIUM FERRITE SPINEL

## 4.1. Introduction

A study of cation stacking faults in the normal spinel $MgAl_2O_4$ has been made by Lewis[34] on crystals grown by the Verneuil method. He found growth faults on {100} planes with a displacement vector $\bar{R} = 1/4\langle 110\rangle$ always at a 45° angle to the fault plane. Planar defects were also found which did not lie on a single crystallographic plane. Glide dislocations were found to be dissociated into two partials on {110} planes with a shear fault in between. Lewis described in detail the configuration of the ions around the fault plane. His method of analysis will be extended here. Baker and Whelan[35] found stacking faults in $Fe_3O_4$, formed by decomposition of $\alpha Fe_2O_3$ in the electron microscope. These stacking faults were lying on {110} planes and they were capable of forming triple junctions. In the spinel $CoFe_2O_4$ on the other hand, De Jonghe[36] did not find any extended faults. However, he did find evidence for a slight dissociation of dislocations.

## 4.2. Results

### 4.2.1. Electron Microscopy--Disordered State

Stacking faults were found in ordered crystals, in the as-received condition. They were also found in partially ordered and disordered crystals, which were annealed above the critical temperature for ordering and quenched. In this section, the stacking faults will be described with reference to the disordered structure only.

Stacking faults were sometimes abundantly present near the surface of a crystal (Fig. 1) but occasionally they were also found in foils taken from the interior. In Fig. 1 some faults are seen edge on

with their trace perpendicular to the operating reflection which is parallel with $[0\bar{1}1]$. This shows that the fault plane is of the {110} type. Trace analysis of other faults in the photograph also show that they lie on {110} planes. This analysis was repeatedly confirmed in other foils. Two examples were found where the fault plane was not {110}, in one case it was (112) and in another (123). These were the only two exceptions found. Notice also that the faults often form three-fold junctions.

The faults can be identified by the symmetry properties of the fringes (for a review see Ref. 37).

The contrast at these faults show $\alpha$ fringes, as they are symmetrical in bright field. In fact, for spinel reflections, and these are the only ones to be discussed in this section, the faults have all the properties of $\pi$ faults, which were derived by Van Landuyt, et al.[38] Characteristically at parallel overlapping faults fringes disappear e.g., at A in Fig. 1 and at intersecting and overlapping faults fringes remain continuous and parallel with the projected line of intersection e.g., at B in Fig. 1.

Figure 2 shows three faults meeting along a line under different diffracting conditions. This set of diffraction experiments allows one to derive uniquely the displacement vector. A fault is invisible when $\bar{g}\cdot\bar{R}$ is an integer, where $\bar{g}$ is the operating reflection and $\bar{R}$ is the displacement vector characterizing the fault. However, one can always add a lattice vector to the displacement vector without altering the physical configuration around the fault. The integer is thus in fact not uniquely determined. When we find three reflections for which the fault is out of contrast we can write three equations:

$$\bar{g}_i \cdot \bar{R} = n_i \qquad i(1,\ 2,\ 3) \tag{1}$$

where $n_i$ must be zero or an integer.

In order to keep the integers on the right hand side completely arbitrary, it is necessary to restrict the $\bar{g}_i$ used in these equations to the lowest order $\bar{g}$ along a systematic row for which a fault goes out of contrast. Otherwise, one restricts the values of the integers e.g., if $\bar{g}_i \cdot \bar{R} = n_i$ then $(2\bar{g}_i) \cdot \bar{R} = 2n_i$ and the integer on the right hand side can only be even.

At high voltages, it is not always simple to determine along a systematic row of reflections the lowest order reflection for which the fault goes out of contrast. Because of dynamical interaction between lower and higher order reflections one may observe a fault, although the phase angle $\alpha = 2\pi\bar{g} \cdot \bar{R}$ is zero for the reflection which is used to form the dark field image.

In order for the Eq. (1) to have a solution, it is necessary that the three vectors $\bar{g}_i$ are linearly independent. One can furthermore predict the following properties of the solutions of Eq. (1), where the $n_i$ are now arbitrary integers: (i) Every lattice vector will be a solution of these equations. This solution is of course a trivial one. (ii) If $\bar{R}$ is a solution of the system then $-\bar{R}$ is also a solution, and these two solutions are not necessarily equivalent unless the difference between the two vectors (viz, $2\bar{R}$) is also a lattice vector. (iii) A linear combination of two solutions is also a solution.

For the stacking fault marked A in Fig. 2 we can write the following equations:

($\bar{R}$ = [uvw] and p,q,r are zero or integers) .

$$u - 3v + w = p$$

$$u + v - 3w = q$$

$$u - v - w = r$$

The solution of these equations yields:

$$\bar{R} = \left[\frac{-p-q+2r}{2} \ , \ \frac{-2p-q+r}{4} \ , \ \frac{-q-r}{4}\right]$$

For p = 1, q = 1 and r = 0 this yields:

$$\bar{R} = \left[\bar{1} \ , \ \frac{\bar{3}}{4} \ , \ \frac{\bar{1}}{4}\right] = [\bar{1}00] + \frac{1}{2}[0\bar{1}\bar{1}] + \frac{1}{4}[0\bar{1}1]$$

The first two vectors at the right hand side are lattice vectors (the lattice is fcc). Thus the smallest displacement vector describing the fault is $\bar{R}$ is $1/4[0\bar{1}1]$ which is perpendicular to the fault plane. This type of analysis has been repeated many times and for all faults the displacement vector was found to be the $1/4\langle 110\rangle$ type with the displacement vector perpendicular to the fault plane.

Figure 2 allows the verification to be made for the Burgers vector of the dislocation confining fault A. A screw dislocation is out of contrast when $\bar{g}\cdot\bar{b} = 0$. The dislocation is out of contrast for $\bar{g} = 1\bar{1}\bar{1}$ and $\bar{g} = 022$. Hence, $\bar{b}$ is parallel with the direction given by the cross product of these two vectors i.e., the $[0\bar{1}1]$ direction. In general, a dislocation confines a region of a crystal which is displaced with respect to the rest of the crystal. From the analysis of the stacking fault we have shown that the displacement is $1/4[0\bar{1}1]$ + a lattice vector. From the $\bar{g}\cdot\bar{b}$ analysis this can be reduced now to

$1/4[0\bar{1}1] + \frac{n}{2}[0\bar{1}1]$. The Burgers vector of the dislocation will be the shortest one of these, hence $\bar{b} = \pm 1/4[0\bar{1}1]$.

4.2.2. Crystallographic Study of Cation Faults in Spinel

In this section an analysis will be made of the configuration of the ions around the fault plane for different orientations of the plane with respect to the displacement vector.

All possible orientations of a $1/4\langle 110\rangle$ displacement vector with respect to the {100}, {110} and {111} planes have been investigated. These are the most important fault planes predicted or found in spinels. Throughout the discussion, the spinel structure will be idealized so that the anions form a perfect cubic closed packed lattice. The analysis will be done for a general spinel structure $AB_2O_4$. Assuming ideal stoichiometry in a normal spinel the average charges of the cations are $A^{2+}$, $B^{3+}$. In an inverse spinel the average charges are $A^{3+}$, $B^{2.5+}$. In a mixed spinel intermediate values of these charges will be found depending on the cation distribution.

A model of a fault can be constructed as follows: starting out from a perfect crystal one choses the location of the fault plane. It is better to chose this location between ionic layers so that it is clear which ion belongs to which part of the crystal. If the displacement vector does not lie in the plane of the fault a slice of material with thickness $\bar{n}\cdot\bar{R}$ ($\bar{n}$: unit vector normal to the fault plane) has to be removed before the two parts can be joined by displacing one with respect to the other over the vector $\bar{R}$. The resulting ionic configuration for a number of faults is depicted in Figs. 3 through 7.

A first question which will be relevant to the subsequent development is: does a particular fault leave an initially stoichiometric crystal stoichiometric? The answer will be yes when no material has to be removed to create the fault i.e., $\bar{R}\cdot\bar{n} = 0$, or when the slice of material removed contains the species making up the crystal in stoichiometric proportions. This problem has been investigated for each orientation of the fault plane and the results are summarized in column 1 of Table I. It can be seen that all various possible fault vectors in relation to the fault planes have been considered. In order to derive these results it is necessary to study the stacking of the ions in different directions in particular the composition in each layer of ions has to be determined.

In ⟨100⟩ directions the centers of the ions line up in planes parallel with {100} planes and spaced a distance $a_o/8$ apart. The arrangement of the cations in these planes is shown in Figs 3 through 6. Choosing in each plane an identical two dimensional unit cell (see Fig. 4), one can determine the composition in each plane. The sequence is $B_2O_4/A/B_2O_4/A$. . . In order to create a {100} 1/4⟨110⟩ type stacking fault it is necessary to remove two of these planes. Hence, the slice of material to be removed is stoichiometric.

A projection of the structure on {110} is shown in Fig. 7. The composition of successive planes is:

$$ABO_2/BO_2/ABO_2/BO_2/ \ . \ . \ .$$

The planes are spaced a distance $a_o\sqrt{2}/8$ apart. When a {110} 1/4⟨110⟩ fault is created two of these layers have to be removed. The composition of the composite layer is $AB_2O_4$. Hence, creation of this fault leaves a

stoichiometric crystal stoichiometric.

A {110} 1/4⟨101⟩ fault has a shear component and this requires removal of only one of the {110} planes. Removal of an $ABO_2$ layer leaves the crystal cation deficient and with an excess of B compared to A. Moreover, whether the spinel is normal or inverse, the fault will acquire a net negative charge. Unless some ions can take a different valence, this type of fault will not be formed. Removal of a $BO_2$ layer leaves the crystal anion deficient, with an excess of A compared with B, but it leaves the fault positively charged.

A similar analysis has been performed for faults of the {111} 1/4⟨110⟩ type. The stacking on {111} planes has been described in detail by Hornstra.[39] He used an extended abc notation to present the position of each ion. The result is given in Table II together with the composition of an identical two dimensional unit cell in each plane. The distance between the planes is $a_o\sqrt{3}/24$ and some of these planes may be empty. The cations occur in two layers. One contains the octahedral ions in the so called kagomé arrangement.[40] The two neighboring planes of the kagomé plane are empty. The other layer is mixed layer containing both tetrahedral and octahedral ions and is spread out over three planes. In order to create a 111 1/4 110 fault, four of these planes have to be removed. The composition of the complete slice of material depends on the exact position of the fault plane. If a plane of oxygen ions forms the boundary then either a complete kagomé

layer (composition $B_3O_4$) or a mixed layer (composition $A_2BO_4$) is to be removed. If a $B_3O_4$ layer is removed then the fault will be negative if the spinel is inverse and will be positive if the spinel is normal. Hence, for a specific distribution of the cations it is possible that this non-stoichiometric fault is neutral. The case of removal of a mixed layer is analogous. If the fault plane breaks up a mixed layer then the composition of removed material will be $AB_3O_4$ or $ABO_4$. In both cases, however, the fault created would be electrically charged.

It is noted here that each non-stoichiometric fault has its complement. The position of the fault plane is the same for both and so is the displacement vector. It will not be possible to determine by conventional electron microscopy techniques what kind of faults one deals with. One needs some other information e.g., the electro-neutrality condition, or the exact local chemical composition of the crystal.

Faults have always been modeled here as intrinsic faults (removal of material). In the present case, with a 1/4⟨110⟩ displacement vector one arrives at identical ionic configurations if the faults are modeled as extrinsic ones.

A 1/4⟨110⟩ vector is a lattice vector of the oxygen sublattice. Hence, only the stacking of cations will be affected and the faults can be called "cation stacking faults". It also follows that a 1/4⟨110⟩ vector will connect interstitial sites with the same coordination in the oxygen fcc sublattice. Hence, a 1/4⟨110⟩ vector cannot change the coordination of the cation from octahedral to tetrahedral or vice versa. Moreover, in the case of the octahedral interstices, sites connected by a 1/4⟨110⟩ vector are also nearest neighbor sites. In the perfect

spinel structure, some of these adjacent octahedral interstices are already occupied, so that at a 1/4⟨110⟩ type fault these ions cannot be brought closer together. Only the distance between an octahedral cation and a tetrahedral cation or between two tetrahedral cations can be affected. As was pointed out by Lewis[34] one can describe these cation faults as anti-phase boundaries, between anti-phase domains within which the partial filling of interstices with cations has stated at different points.

It will be shown now that a {110} 1/4⟨110⟩ fault is the fault with the lowest energy in an overall stoichiometric crystal. There are two major contributions to the surface free energy of a stacking fault in these ionic structures. (i) There can be a change in the distance between first, second, third, etc . . . nearest neighbors. (ii) There can be a change in the number of first, second, third etc . . . nearest neighbors.

The latter contribution will be largely ignored here. A detailed analysis of the change in number of nearest neighbors for every fault plane would be quite complicated. This analysis would amount to an actual calculation of the energy of each type of fault. This is outside the scope of this work. Instead, attention will be focused on the relative energies of each fault type and it will be sufficient to study how the intercation distances are changed for each orientation of the fault plane. As was pointed out above, the coordination of the cations with respect to the anions remains unchanged. Only the change in coordination of the cations relative to each other needs to be studied. It is useful here to consider the spinel structure as a stacking of

coordination polyhedra with cations in the centers and oxygen ions at the corners. In the perfect spinel structure, the octahedra share edges with four other octahedra and share corners with six tetrahedra. The tetrahedra do not touch each other. Whenever these polyhedra share elements with a higher dimensionality than in the perfect structure, then the distance between the cations at the center of the polyhedra will be smaller. In spinels, these cations are highly charged. The strong repulsion between cations is expected to make up the major part of the surface free energy of the fault. The shorter the intercation distance, the higher the surface free energy of the fault will be. The actual ionic configuration depends on the relative orientation of $\bar{R}$ and the fault plane. This has been studied with the help of projections of the structure and a three dimensional model.* The results have been summarized in Table I, columns 2 to 5.

From a model of a {100} 1/4⟨110⟩ fault (Fig. 3) it can be deduced that across the fault plane tetrahedra will share corners and octahedra will share faces with tetrahedra. The latter point was missed by Lewis,[34] who described a model for a shear fault on {100}, pointing out correctly that tetrahedra would share edges across the fault plane. However, there is another possible ionic configuration when one chooses another ⟨110⟩ direction as the shear direction (see Fig. 4) or another position of the

*The following part of the analysis can be more easily understood with the help of a three dimensional model of the spinel structure. These models are available commercially e.g., by LAPINE, 6011 South Knox Avenue, Chicago, Illinois 60629.

fault plane. Such a configuration is also one with high energy, as octahedra and tetrahedra share faces across the fault plane. Figure 5 depicts a shear fault on {110}. Again across the fault plane octahedra and tetrahedra share faces. This reduces the distance between octahedra and tetrahedra from $0.414a_o$ in the perfect structure to $0.217a_o$ in the faulted structure i.e., a 49% reduction.

In Figs. 6 and 7 a model of a {110} 1/4⟨110⟩ fault is represented. The octahedra and tetrahedra retain their distance. The distance between tetrahedral ions has been reduced from $0.434a_o$ to $0.354a_o$. This is only a reduction of 18% and $0.354a_o$ is exactly the shortest distance between octahedral ions in the spinel structure.

Faults of the {111} 1/4⟨$\bar{1}$10⟩ type were discussed by Hornstra[39] who also pointed out that octahedra and tetrahedra have a face in common at the fault plane. For fault planes were the stoichiometry is not conserved the ionic configuration will also depend on the particular species one has removed to create a fault. For the faults of type {110} 1/4⟨101⟩ and {111} 1/4⟨110⟩, fault planes can be found with low energy from the point of view of cation separation. However, in an overall stoichiometric crystal an equal surface area of the complementary fault plane has to exist. The latter has then a very high energy. Moreover, some of these faults have to be excluded if they would leave the fault plane electrically charged.

It can be seen from Table I that a {110} 1/4⟨110⟩ fault will have the lowest energy in a stoichiometric crystal. For this particular orientation of the fault plane only the distance between the tetrahedral ions is changed. But this distance does not become smaller than the

smallest intercation distance in the spinel structure.

### 4.3. Summary of Facts

It has been found experimentally that lithium ferrite contains faults on {110} planes. From contrast experiments it was shown that the displacement vector characterizing these faults is 1/4⟨110⟩ with this vector always perpendicular to the fault plane. From the properties of the spinel structure it follows that these faults affect only the cations. From geometric and energetic arguments it has been shown that in a stoichiometric spinel a {110} 1/4⟨110⟩ fault has the lowest surface free energy. The stoichiometry of the crystal is not affected by the introduction of such a fault.

### 4.4. Discussion

The frequent occurence of three-fold junctions in Fig. 1 can now easily be explained, if we allow only faults with the a displacement vector perpendicular to the plane. It is clear that such a fault cannot simply change planes. This would necessarily involve a dislocation (Fig. 7a). An example of this can be seen at C in Fig. 1, where one of the faults is edge-on. However, when three faults meet along a line (necessarily a ⟨111⟩ direction) there is no need to introduce a dislocation, as a Burgers circuit around the line would yield a zero displacement (Fig. 7b). Cation faults forming three-fold junctions were also observed in magnetite by Baker and Whelan.[35] These faults are presumably of the same type as the ones found here. In contrast a (100) 1/4[110] fault, found in $MgAl_2O_4$ can easily change to the (010) plane without the need for a dislocation.

A central assumption in our analysis of cation faults in spinels has been that the crystal is stoichiometric. Once this restriction is removed one cannot analyse the faults anymore using as a model a rigid structure of point atoms. Hence, one cannot predict from simple geometric arguments what the fault plane with the lowest energy will be. It is conceivable that point defects which necessarily have to be introduced in a non-stoichiometric crystal, will preferentially be found at the fault plane. For example, in the case of a {100} 1/4⟨110⟩ fault (Fig. 3) vacancies on tetrahedral sites could preferentially occupy those tetrahedral sites which are simultaneously close to an octahedral site and a tetrahedral site. This would lower drastically the free energy of the fault. The observations on $MgAl_2O_4$ were done indeed on a crystal with excess $Al^{3+}$, which is expected to introduce excess vacancies on tetrahedral sites.

In the case of $LiFe_5O_8$, a characterization of the point defect structure is hampered by the fact that: (i) no reliable method of analysis for lithium content exists; (ii) one needs the exact oxygen content of the sample, because iron can occur as either divalent or trivalent ions. In the present case, although chemical analysis indicated a lithium deficiency in the crystal, this does not necessarily prove that the crystals contain a large concentration of extrinsic vacancies, as a lithium-deficient crystal can be derived from the stoichiometric one by the substitution of $2Fe^{2+}$ for $(Fe^{3+} + Li^{+})$.

Other factors which may lead to a variation in the observed fault plane are the composition of the spinel and the thermal history. For instance, in flux grown $CoFe_2O_4$ no extended cation faults were observed.[36]

In $MgAl_2O_4$ crystals, faults were observed which did not lie on single crystallographic planes.[34] The latter were grown by the Verneuil process, a method of crystal growth which involves a steep temperature gradient. In contrast the lithium ferrite crystals used in this work were grown under near equilibrium conditions.

# 5. DOMAINS IN ORDERED LITHIUM FERRITE-ENANTIOMORPHISM

## 5.1. Introduction

When a structure belongs to a spacegroup which does not contain a symmetry operation of the second sort, that is an operation which does not involve an inversion or a reflection, then it can exist in either a right-handed or a left-handed form. In some cases, these two forms have different spacegroups; that is, either one of an enantiomorphous pair of space groups. With ordinary X-ray diffraction techniques it is impossible to distinguish between these two enantiomorphous forms. It is necessary to include anomalous scattering in the calculations and often very accurate intensity measurements are necessary. The use of anomalous scattering of X-rays to determine the absolute configuration of a structure has been reviewed by Ramaseshan.[41] Recent contributions to this field include the use of the shape of X-ray intensity spectra[42] and applications of the Kossel effect.[43]

These X-ray methods have their limitations. The structure should contain at least two different species, one of which should be an anomalous scatterer. The latter condition cannot always be fulfilled with commonly available X-ray wavelengths, for instance, if a structure contains only light elements. Iwasaki[44] has shown that there may be some, so far imaginary, non-centrosymmetric structures, for which Friedel's law holds even with anomalous dispersion. In addition, one would have to be sure that both forms of the structure do not coexist on a very fine scale viz smaller than the diameter of an X-ray beam, within an apparent single crystal. This will depend on whether or not it is possible to have a low energy interface between the two structures,

when the crystal axes in both remain parallel.

In this section it will be shown that if both enantiomorphous forms do occur in the form of very small domains, the presence of the right and left-handed forms can be confirmed using contrast experiments in the electron microscope. Two different methods have been used, the first method consists of an analysis of the interface between the two structures. This interface can be described by a set of geometrical operations which converts the structure on one side into the structure on the other side of the interface. Using simple contrast experiments it can be ascertained whether or not the operations characterizing the interface contain an inversion operation. A similar method of analysis was used by MacLaren and Phakey[45] in a study of Brazil twinning in quartz. The second method which can be used to confirm the results of the first, takes advantage of a violation of Friedel's law in electron diffraction. Exceptions to Friedel's law in electron diffraction were first observed by Thiessen and Moliere[46] and later by Miyake and Uyeda.[47] A theoretical discussion of Friedel's law in n-beam dynamical theory was given by Fujimoto,[48] Cowley and Moodie[49] and recently by Serneels, Snykers, Delavignette, Gevers and Amelinckx,[50] who specifically considered the contrast between domains related by an inversion operation in non-centrosymmetrical crystals.

## 5.2. Structural Information

When disordered lithium ferrite orders, its spacegroup symmetry is lowered from Fd3m to $P4_132$ or its enantiomorph $P4_332$. The atomic coordinates for the ions used in this work were given by Braun[6] using the equivalent positions for $P4_332$ (No. 212 International Tables for X-ray crystallography, 1965): 4 Li at (b); 12 Fe at (d) with x = 3/8;

8 Fe at (c) with x = 0; 24 Oxygen at (c) with x = 1/8, y = -1/8, z = 1/8, 8 Oxygen at (c) with x = 3/8. Small corrections for these coordinates were neglected i.e., we assumed that the disordered structure is an ideal spinel structure. The complete set of coordinates of the octahedral sites is given in Table III. A projection of these sites on the (100) plane is given in Fig. 9.

Considering now one spacegroup only, it can be seen from Fig. 9 that the set of octahedral sites can be divided into four subsets, one of which contains only lithium ions and the other three only iron ions. When ordering sets in, the lithium ions can occupy any of these four subsets. After ordering, the single crystal is fragmented into domains in a way similar to ordered metallic phases (e.g., see Marcinkowski[51]). Within each domain, the lithium ions will occupy only one subset and at the boundary between domains they will be out of phase. These boundaries can be described by the vector which translates the lithium ions from one subset to another. A 1/2⟨110⟩ type vector is a lattice vector of the disordered structure, hence, a translation of the ordered structure over this vector does not affect the oxygen ions or iron ions in tetrahedral sites, but it does transfer the Li ions from one subset to another. This holds for either one of the spacegroups.

So, there are actually eight different subsets out of the 16 octahedral sites which the Li ions can occupy, and it is possible to have a boundary between any pair of these. The eight arrangements are enumerated in Table IV. The arrangements 1L and 1R have been taken rather arbitrarily as "basic" arrangements for $P4_332$ and $P4_132$ respectively. These two arrangements can be brought into coincidence with one another

by an inversion through the point (5/8,5/8,5/8), hence, the boundary between these two arrangements will be called an inversion boundary. On the other hand, a boundary between 1L and 2R would not only involve an inversion through (5/8,5/8,5/8) but also a translation over a vector 1/2[110].

This description of the boundaries is not unique. In principle, each boundary involving an inversion can be described as a pure inversion boundary by proper choice of the inversion point. Here the inversion point is considered to be fixed. In the context of this paper "inversion" means inversion through the point (5/8,5/8,5/8). The boundaries could also be described by means of a reflection operation, for instance with respect to the (110) planes, which may or may not be accompanied by a translation.

One could have a total of 28 boundaries between the eight possible arrangements. However, only seven boundaries, distinct in the geometrical operations characterizing them, can occur. These boundaries are indicated schematically in Fig. 10. There are three translation boundaries, one inversion boundary and three boundaries described by an inversion and a translation. All 28 boundaries are enumerated and classified in Table V.

## 5.3. Contrast in the Electron Microscope

### 5.3.1. Contrast at Domain Boundaries

It is useful to consider here the two beam dynamical theory of contrast at a stacking fault in crystals (e.g., see Whelan and Hirsh[53] and Hirsch, Howie, Nicholson, Pashley and Whelan[52]). The equations for the faulted crystal can be derived from those of the perfect crystal simply by modifying the Fourier coefficient of the crystal potential

in the bottom part of the crystal by a phase factor $\exp(i\alpha)$, i.e.,

$$V_g^b = V_g^t \exp(i\alpha) \tag{1}$$

where b indicates the bottom of the crystal and t indicates the top (facing the electron beam). $\alpha = -2\pi\bar{g}\cdot\bar{R}$, where $\bar{R}$ is the displacement of the bottom relative to the top and $\bar{g}$ is the reciprocal lattice vector corresponding to the reflection excited. It is understood here that the potential of the top of the crystal $V^t(\bar{r})$ and the potential of the bottom $V^b(\bar{r})$ have both been referred to the same origin. Equation (1) implies that:

$$F_g^b = F_g^t \exp(i\alpha) \tag{2}$$

This equation yields another interpretation for the phase angle $\alpha$: $\alpha$ is the difference between the phase angles in the structure factor expressions for the top and bottom of the crystal, calculated with respect to a common origin.

In the case of a boundary between a left-handed and a right-handed crystal, we can write quite generally the following expression for the structure factor:

$$F_g^\ell = |F_g^\ell| \exp(i\alpha_g^\ell) \quad F_g^r = |F_g^r| \exp(i\alpha_g^r)$$

In particular, for the moduli of the structure factor it follows regardless of choice origin:

$$|F_g^\ell| = |F_g^r|$$

Hence, it follows that:

$$F_g^\ell = F_g^r \exp(i(\alpha_g^\ell - \alpha_g^r))$$

or

$$F_g^\ell = F_g^r \exp(i\alpha) \tag{3}$$

with

$$\alpha = \alpha_g^\ell - \alpha_g^r \tag{4}$$

Considering now a boundary between the two enantiomorphs with the right-handed structure at the top of the crystal facing the electron gun and the left-handed structure at the bottom, Eq. (3) implies that

$$V_g^\ell = V_g^r \exp(i\alpha) \tag{5}$$

Hence, the relationship between the crystalpotential in the two parts of the crystal on either side of this boundary is the same as in the case of a stacking fault. The results of the two beam dynamical theory of contrast at a stacking fault apply equally well to this boundary. A boundary between two enantiomorphs will be imaged as $\alpha$ fringes where $\alpha$ is now equal to the difference in the phase angle of the structure factor expression calculated with respect to the same origin. This phase difference is independent of the actual choice of origin.

In the dynamical theory of contrast the assumption is usually made that the crystal is centrosymmetric so that one can write $V_g = V_{-g}$ (or $F_g = F_{-g}$). In a two beam case this assumption is not really necessary as one is free to chose the origin so that for a particular beam $F_g^t = F_{-g}^t = F_g^{t*}$ which means that in the example above $\alpha_g^r = 0$. It is

clear that this approach to the contrast problem at an inversion boundary will not be valid in the case of a many-beam situation, because it is then not possible to chose an origin so that the condition $V_g = V_{-g}$ is simultaneously fulfilled for all the beams involved.

Using a simple structure factor program, the values of $\alpha$ were calculated for each of the seven boundaries which occur in ordered $LiFe_5O_8$. The atomic coordinates for the iron and lithium ions on the octahedral sites given in Table IV were used. The results are shown in Table VI. In the case of translation boundaries the value of $\alpha$ is also equal to $-2\pi\bar{g}\cdot\bar{R}$. Wherever $\alpha = 0$ or $2\pi$, a domain boundary will be out of contrast. For reflections of the type 110, 211, 103, 123, $\alpha$ takes the value 0, $\pi$. For reflections of the type 102, 302 $\alpha$ takes the value 0, $\pi$ for translation boundaries but only $\pm\pi/2$ for inversion boundaries. For all spinel reflections $\alpha = 0$ and the boundaries should be out of contrast.

5.3.2. Contrast Between Domains

In a second method, by which the presence of two enantiomorphous structures can be verified, one takes advantage of the violations in Friedel's law which take place in electron diffraction in certain multiple beam situations. What is meant by a violation of Friedel's law is that +g and -g do not have the same intensity even when the excitation errors are the same. At an inversion boundary, when +g is operating in one part of the crystal, -g is operating in the inverted part, with exactly the same excitation. When Friedel's law is violated then the domains should show up with different intensity. This situation is studied by Serneels, et al.[50] and they concluded the following: (i) A multi-beam condition is necessary to observe any contrast at all. (ii) Friedel's law holds

for the direct beam in a general multiple beam situation. It does not hold in general in dark field. (iii) The difference in intensity depends strongly on the thickness of the crystal. (iv) If the only reflections excited belong to a zone axis along which the crystal displays a center of symmetry in projection, no contrast should be observed in dark field.

## 5.4. Results

### 5.4.1. Translation and Inversion Domains

From systematic extinctions in the precession photographs it was confirmed that the spacegroup of the disordered structure is Fd3m. The precession photographs of the ordered compound showed the presence of systematic extinctions required for the spacegroups $P4_132$ and $P4_332$. The non-systematic extinctions in these photographs could be accounted for by the atomic positions given by Braun.[6]

Figure 11 shows a series of transmission electron micrographs taken under a variety of diffraction conditions. Figure 11a was taken under conditions approaching a two beam case as the $0\bar{2}4$ and $02\bar{4}$ reflections are not allowed. Figures 11b, 11c and 11d were taken with a systematic row of reflections operating with the indicated reflection on the Ewald sphere. Although the presence of the systematic beams will alter the detail of the contrast at the boundary, it will not affect the visibility criteria derived for two beam conditions. The visibility or invisibility of the boundaries marked by a lower case letter in Fig. 11a has been tabulated in Table VII. Comparison of these results with the calculations given in Table VI allows one to identify each of the boundaries with one of the seven types of boundaries possible. This identification is made

in the last column of Table VII.

The internal consistency of the method of analysis can be checked by labelling each domain as follows: because at present, these electron microscopic methods do not yet allow the determination of the absolute configuration, it was assumed that the domain which runs vertically through the micrograph has a left-handed $P4_332$ arrangement. It was also assumed that it was the "basic" 1L arrangement. The latter assumption is equivalent to choosing an origin. Once these assumptions are made, the arrangements of all the other domains can be found through the character of their boundaries derived in Table VII, and the use of Table V. This was done in Fig. 11a. This labelling of domains provides a check, on the identification of the boundaries e.g., if a is a boundary between 1L and 3R and b is a boundary between 3R and 4R, then clearly the character of c is fixed and c has to behave as a 1L -4R boundary, i.e., $I + T_3$. This has indeed been found by contrast experiments (Table VII). Hence, a complete internally consistent picture is obtained of the relationships between the domains.

An independent check on these results is provided in Figs. 11e, 11f and 11g. The same area was imaged here under multi-beam conditions (Fig. 11g), hence, one may expect violations of Friedel's law at inversion boundaries. The foil was wedge-shaped with thinner parts at the bottom of the pictures. The fringes in Fig. 11e running from right to left are thickness fringes. These remain continuous across the boundaries in the bright field picture. In dark field, however, these fringes change color at some boundaries (e.g., at a and c) but remain continuous across others (e.g., at j and g). The latter ones may be

expected to be translation boundaries whereas the first should be inversion boundaries. Comparison with Fig. 11a shows that these boundaries are the same ones for which the first method showed that an inversion was involved.

Figure 12 provides another example where the two enantiomorphous structures can be distinguished by a difference in background intensity. This specimen was chemically thinned and some etching had occurred at the boundaries. The presence of two strong "accidential" reflections was sufficient to provide a very strong contrast between enantiomorphous domains e.g., at A and B. There is no difference in background intensity across translation boundaries e.g., at C and D.

The size of the domains depends on the thermal history of the sample. In the as received crystals, the domain size was of the order of 5μ (Fig. 13). In Fig. 11 and Fig. 12 the sample had been annealed at 850°C and was then slowly cooled in the furnace (approximately 100°C/hr). The sample in Fig. 14 had been quenched from 950°C in water, then annealed at 650°C for 100 min and shows a substantially smaller domain size.

5.4.2. Stacking Faults in Ordered Lithium Ferrite

In Section 4.2 it was shown that the cation faults can be described with respect to the spinel structure with a displacement vector 1/4⟨110⟩ plus a spinel lattice vector. Upon ordering, the crystal looses some of its translational symmetry elements, the lattice reduces from face centered cubic to primitive cubic; and the fcc translation vectors of the type 1/2⟨110⟩ are no longer lattice vectors. Hence, any combination of the displacement vector, with respect to the fcc lattice i.e., 1/4⟨110⟩ with a 1/2⟨110⟩ vector yields a possible displacement vector for cation

faults in the ordered structure. Some of these variants, however, are related by a translation vector of the primitive lattice, so that only four distinctively different displacement vectors can be generated, e.g., for a fault on the (110) plane we find $\bar{R}_1 = 1/4[110]$ $\bar{R}_2 = 1/4[\bar{1}\bar{1}0]$ $\bar{R}_3 = 1/4[\bar{1}1\bar{2}]$ $\bar{R}_4 = 1/4[1\bar{1}2]$. All other variants one may derive by combining 1/4[110] with any 1/2⟨110⟩ will differ from one of these four only by a primitive cubic lattice vector. One can distinguish between the displacement vector of the 1/4⟨110⟩ type and the 1/4⟨112⟩ type by contrast experiments, using of course, superlattice reflections for this purpose. The distinction between +R and -R can be made by a determination of the sign of $\alpha$ when $\alpha = \pm\pi/2$.

An example of a 1/4⟨112⟩ type fault is given in Fig. 15. Figure 15a shows that the fault vector cannot possibly be perpendicular to the fault plane as $\bar{g}\cdot\bar{R}$ would then be zero. Figure 15b confirms that the fault vector is lying in the plane of the fault. However, the analysis is not always as straight forward as in this example, because in the ordered structure an inversion can occur at these cation stacking faults, as will be shown below. It is clear that a translation boundary with $\bar{R}$ = 1/2⟨110⟩ can always join the cation stacking fault, without the need for a dislocation at the junction. At this junction the cation stacking fault may change character from 1/4⟨110⟩ type to 1/4⟨$\bar{1}$12⟩ type.

Figure 16 shows three stacking faults on {110} planes meeting along a line. The displacement vector of these faults was determined as 1/4⟨110⟩ plus a spinel lattice vector. The boundary 4 joining fault 1 is a translation boundary. The contrast in Fig. 16d can be explained only if faults 1 and 2 are simultaneously boundaries between the left

and right-handed structure. The displacement vectors of these faults are: $\bar{R}_{1a} = 1/4[101]$, $\bar{R}_{1b} = 1/4[\bar{1}0\bar{1}]$, $\bar{R}_2 = 1/4[110]$. For $g = \bar{1}0\bar{2}$, this yields for the phase angle: $\alpha_{1a} = \pi/2$, $\alpha_{1b} = -\pi/2$ and $\alpha_2 = -\pi/2$. Hence, If these faults were simple translation faults, they should be visible as $\alpha$ fringes with $\alpha = \pm\pi/2$. If these faults also included an inversion operation then a phase angle of $\pm\pi/2$ would be added (see Table VI). Taking the plus sign yields: $\alpha_{1a} = \pi$, $\alpha_{1b} = 0$ and $\alpha_2 = 0$. Hence, the b part of fault 1 and fault 2 will be invisible. This matches the observations.

Additional evidence that stacking faults can also serve as the boundary between enantiomorphous forms is given in Fig. 17. Figure 17a was taken under the diffraction conditions shown in Fig. 17b. Figure 17c shows that the fault ABC seen edge on in 17a is indeed a stacking fault. Analysis of the boundaries a and b showed that they were pure inversion boundaries. The difference in background contrast at A and C indicates that an inversion takes place at the stacking fault. However, there should not be any difference in background intensity at B. This is indeed observed.

Figure 18 shows an interesting interaction between a translation boundary and a cation stacking fault. The translation boundary lies approximately on the (101) plane and is terminated by a dislocation with Burgers vector 1/2[101] (Fig. 18a). This dislocation, however, is dissociated into two partials with a 1/4[101] Burgers vector and a fault in between with the same displacement vector. The use of a higher order reflection in Fig. 18c reduces the image width of the dislocation, so that they are better resolved.[55]

## 5.5. Discussion

The domain size in the ordered crystal depends on the heat treatment but is usually of the order of 1μ or smaller and hence, well below the diameter of an X-ray beam. It is clear that a very fine intergrowth of the two enantiomorphous structures would give rise to a spurious center of symmetry in diffraction even when an X-ray wavelength is used for which iron is a strong anomalous scatterer. The success of the electron microscopic method does not depend on the presence of a particular atomic species in the compound. The method should also be applicable for structures containing only lightweight elements.

In the multibeam method, the contrast in dark field arises due to a complex interaction between n beams. However, one cannot show in general that the difference in intensity between the inverted domains will be large enough to be detectable. This difference in intensity will depend on the details of the structure, the thickness of the sample and the diffraction conditions. It is shown by Serneels et al.[50] that for very thick foils the contrast will be destroyed by absorption.

The analysis of an inversion boundary using different g vectors should be applicable to all crystals in which enantiomorphous domains occur. The success of this method hinges on the fact that there is a difference in phase angle of a particular reflection for the two enantiomorphous structures when both are referred to the same reference frame. Reflections for which this phase angle difference is not equal to zero can always be found. This method has the additional advantage that it yields a complete description of the interface between the two structures. Not only can it be established that an inversion operation

is involved at the boundary but any additional translation can be determined as well. In general, these translations are not known *a priori*. In the case of ordered $LiFe_5O_8$ a precise description of the domain structure can be given because the ordered structure is derived from the relatively simple spinel structure. This is the reason why lithium ferrite forms an ideal case to illustrate the use of these electron microscopic techniques.

For all practical purposes it might be sufficient to establish the presence of the two enantiomorphous forms within an apparent single crystal. The microscopic methods described in this paper have not yet been extended to determine the absolute configuration of the structure in a part of the crystal. In principle, this possibility exists. In the case of the multibeam method, one should be able to predict using a many-beam dynamical theory for non-centrosymmetric crystals, which form whould show up bright in dark field for a given crystal thickness and diffraction conditions. In general, an electronic computer would have to be used for this. The problem is completely analogous to the absolute determination of the orientation of a non-centrosymmetrical crystal, which has reflection symmetry. This problem has been solved for hexagonal CdS by Goodman and Lehmpfuhl,[54] who used a convergent beam technique and a multiple slice calculation for n-beam diffraction. In the case of the interface analysis, it should be possible to predict for an interface inclined with respect to the beam, which form is at the top of the crystal facing the electron gun. This can only be done when the difference in phase angle $\alpha$ is different from $\pi$. In the case of ordered lithium ferrite this is the case for reflections of type 012 or

203 when $\alpha = \pm\pi/2$. The problem is then reduced to a determination of the sign of $\alpha$ and is analogous to the determination of the character of a stacking fault in fcc metals (Hirsch, et al.).[52] A systematic study of this problem for $\alpha = \pi/2$ has not yet been undertaken.

## 6. GENERAL DISCUSSION

From the results of the preceeding section, the following picture can be drawn regarding the crystalline defects in flux grown lithium ferrite crystals. The cation faults were found in crystals which had undergone different heat treatments as well as in crystals in the as grown condition. It is unlikely that these faults are in any way connected with the heat treatments. If they were, e.g., if they were due to thermal stresses during quenching, one would expect shear faults confined by glissile dislocations. From the crystallographic study it is clear that they are not the result of cation vacancy aggregates, although vacancies can interact with them once they are formed. More probably, the faults were formed during growth of the crystals from the melt. The faults can be viewed as antiphase boundaries resulting from an ordering reaction in a disordered structure which can be derived from the spinel structure by randomization of the occupied and vacant interstitial sites. This structure may be an intermediate state during solidification from the melt. The faults would be the results of "growth accidents" during which the filling of interstices started at non-equivalent points in the structure. The fact that faults were found more abundantly near the surface of the crystals is consistent with this, as the probability of these growth accidents occurring increases as the crystal grows.

Initially, the faults may not have been on single, low-index planes, but due to the low cooling rate, they could take a low energy configuration, which was shown to be on the {110} plane with a 1/4⟨110⟩ displacement vector perpendicular to it. Some faults may have annealed out all together,

but in areas with a high fault density a domain structure could be expected as is indeed observed (Fig. 1).

As far as the description of the faults is concerned, a {110} 1/4⟨110⟩ and a {110} 1/4⟨$\bar{1}$12⟩ fault are completely equivalent as these displacement vectors differ only by a lattice vector. In ordered lithium ferrite this is no longer the case. It is clear, however, that during the ordering reaction the Burgers vector of the grown-in dislocation cannot change. Hence, the fundamental character of the faults cannot be changed. Along the fault plane, however, the faults can change from 1/4 ⟨110⟩ type to 1/4⟨$\bar{1}$12⟩ type through interaction with 1/2⟨110⟩ type translation boundaries. The faults can also become the boundary between enantiomorphous forms of the ordered structure.

It has been shown that cation stacking faults in magnetite can effectively pin magnetic domain walls.[2] As lithium ferrite and magnetite are quite similar both structurally and chemically, the same phenomenon can be expected to occur in lithium ferrite. Hence, the distribution and density of these defects will influence the magnetic properties e.g., the initial permeability and coercive force. The fault density can only be controlled during preparation of the compound from the melt, from the vapor or by solid state reactions. These faults can be especially important in the production of thin films which are usually prepared under conditions far away from equilibrium.

It has also been shown in ordered metallic systems that magnetic domain walls can be pinned by antiphase boundaries.[2] It can be assumed that this is also the case in lithium ferrite. There is ample evidence in the literature[8,18-20] that some important magnetic properties are

dependent upon the state of order of the system (see Section 2). There are also indications that a correlation exists between the electrical conductivity of single crystal samples and the domain size in the ordered structure.[56] This domain size can be controlled by the proper heat treatment. No attempt has been made here to study the kinetics of the disorder-order reaction and the domain growth in a quantitative way. This will form the subject of a forthcoming study.[57] In this work, the groundwork has been laid for a correct interpretation of the microstructure in the ordered phase.

## ACKNOWLEDGEMENTS

First of all, the author would like to thank his parents for their understanding and continuous support. He also would like to thank his wife Lutgarde for her patience and her support during the last four years.

The author is also deeply indebted to Professor Gareth Thomas for guiding him through some hazards of a graduate student's life and continuous direction throughout the research project. Thanks are also due to Mr. Don Jurica, for keeping an often recalcitrant microscope running, and to Ms. Margaret Robson for her superb organization of the electron microscope facilities.

The author also wishes to acknowledge Dr. W. F. Müller, for help with the ion bombardment apparatus, Professor M. J. Goringe for a critical reading of part of the manuscript and Dr. L. J. Chen and Mr. Ron Gronsky for useful discussions.

Thanks are also due to the entire technical support staff of the Inorganic Materials Research Division, in particular Mr. Douglas Kreitz (photography) and Miss Jean Wolslegel (technical typing).

This work was done under the auspices of the U. S. Atomic Energy Commission through the Lawrence Berkeley Laboratory.

REFERENCES

1. M. H. Lewis, Phil. Mag. 17, 481 (1968).

2. A. P. Lapworth, J. P. Jakubovics and G. S. Baker, J. de Phys. 32, Suppl. C1-259 (1971).

3. J. Washburn, Electron Microscopy and Strength of Crystals, G. Thomas and J. Washburn, eds. (J. Wiley and Sons, Inc., New York, 1961).

4. S. Amelinckx and P. Delavignette, Electron Microscopy and Strength of Crystals, G. Thomas and J. Washburn, eds. (J. Wiley and Sons, Inc., New York, 1961).

5. M. H. Lewis, J. Billingham and P. S. Bell, Electron Microscopy and Structure of Materials, G. Thomas, R. Fisher and R. Fulrath, eds. (University of California Press, Berkeley, 1972).

6. P. B. Braun, Nature 170, 1123-24 (1952).

7. G. Blasse, Philips Res. Repts. Suppl., No. 3, 1964.

8. Handbook of Microwave Ferrite Materials, W. H. Von Aulock, ed. (Academic Press, 1965).

9. H. P. J. Wijn, E. W. Gorter, C. J. Esveldt and P. Gelderman, Philips Tech. Rev. 16[2], 45 (1954).

10. E. A. Schwabe and D. A. Campbell, J. Appl. Phys. 34[4,pt. 2], 1251 (1963).

11. R. G. West, J. Appl. Phys. 34[4,pt. 2], 1113 (1963).

12. D. B. Rogers, R. W. Germann and R. J. Arnott, J. Appl. Phys. 36[8], 2338 (1965).

13. R. G. West and A. C. Blankenship, J. Am. Ceram. Soc. 50[7], 343 (1967).

14. P. K. Baltzer, U. S. Pat. 3,034,987 (1962).

15. D. H. Ridgeley, H. Lessof and J. D. Childress, J. Am. Ceram. Soc. 52[6], 304 (1970).

16. A. J. Pointon and R. C. Saull, J. Am. Ceram. Soc. 52[3], 157 (1969).

17. G. Bandyopadhyay, Relation of Processing Parameters to the Properties of Lithium Ferrite (Ph. D. Thesis), LBL-2263, Nov. 1973.

18. V. J. Folen, J. Appl. Phys. 29, 378 (1958).

19. A. D. Schnitzler, V. J. Folen and C. T. Rado, J. Appl. Phys. 31, Suppl. 348S (1960).

20. R. T. Denton and E. C. Spencer, J. Appl. Phys. 33, 1300 (1962).

21. E. Kato, Bull. Chem. Soc. Japan 31, 113 (1958).

22. E. Kato, Bull. Chem. Soc. Japan 32, 631 (1959).

23. E. A. Gugenheim, Mixtures (Oxford University Press, London, 1952), p. 101.

24. D. W. Strickler and R. Roy, J. Am. Ceram. Soc. 44, 225 (1961).

25. M. Brunel and F. de Bergevin, C. R. Acad. Sc. Paris 258, 5628 (1964).

26. M. Brunel and F. de Bergevin, Solid State Comm. 4, 165 (1966).

27. K. Yamada and A. Yoshimori, Progress Theoretical Physics 37, 473 (1967).

28. J. G. Allpress, J. Mat. Sci. 6, 313 (1971).

29. M. Schieber, J. Inorg. Nucl. Chem. 26, 1363 (1964).

30. D. J. Barber, J. Mat. Sci. 5, 1 (1970).

31. L. C. de Jonghe and G. Thomas, J. Appl. Phys. 41, 4884 (1970).

32. D. J. Barber, F. C. Frank, M. Moss, J. W. Steeds and I. S. T. Tsong, J. Mat. Sci. 8, 1030 (1973).

33. E. Levine, W. L. Bell and G. Thomas, J. Appl. Phys. 38, 289 (1967).

34. M. H. Lewis, Phil. Mag. 14, 1003 (1966).

35. G. S. Baker and M. J. Whelan, Proc. of the 7th Intern. Congress of Electron Microscopy, Société Française de Microscopie Electronique, 1970.

36. L. C. De Jonghe, Defects and Phase Transformations in Cobalt Ferrites (Ph. D. Thesis), UCRL 20369, Nov. 1970.

37. S. Amelinckx, Modern Imaging and Diffraction Techniques, S. Amelinckx, R. Gevers and J. Van Landuyt, eds. (North-Holland Publishing Co., 1970).

38. J. Van Landuyt, R. Gevers and S. Amelinckx, phys. stat. sol. 7, 519 (1964).

39. J. Hornstra, J. Phys. Chem. Solids 15, 311 (1960).

40. S. Iida, J. Phys. Soc. Japan 12, 222 (1957).

41. S. Ramaseshan, Advanced Methods in Crystallography, S. Ramachandran, ed. (Academic Press, 1964), p. 67.

42. K. F. Burr and J. Woods, J. Mat. Sci. 6, 1007 (1971).

43. O. Brümmer, W. Beier and H. Neiber, phys. stat. sol. (a) 20, K119 (1973).

44. H. Iwasaki, Acta Cryst. A30, 173 (1974).

45. A. C. McLaren, P. P. Phakey, phys. stat. sol. 13, 413 (1966).

46. P. A. Thiessen and K. Moliere, Ann. Phys. 34, 449 (1939).

47. S. Miyake and R. Uyeda, Acta Crystl 3, 314 (1950).

48. F. Fujimoto, J. Phys. Soc. Japan 14, 1558 (1959).

49. J. M. Cowley and A. F. Moodie, Acta Cryst. 12, 360 (1959).

50. R. Serneels, M. Snykers, P. Delavignette, R. Gevers and S. Amelinckx, phys. stat. sol. (b) 58, 277 (1973).

51. M. J. Marcinkowski, Electron Microscopy and Strength of Crystals, G. Thomas and J. Washburn, eds. (Interscience, 1961), p. 333.

52. P. B. Hirsch, A. Howie, R. B. Nicholson, D. W. Pashley and M. J. Whelan, Electron Microscopy of Thin Crystals (Butterworth, 1965).

53. M. J. Whelan and P. B. Hirsh, Phil. Mag. 2, 1121 (1957).

54. P. Goodman and G. Lehmpfuhl, Acta Cryst., A24, 339 (1968).

55. W. L. Bell and G. Thomas, Electron Microscopy and Structure of Materials, G. Thomas, ed. (University of California Press, 1971).

56. O. Van der Biest, unpublished research.

57. O. Van der Biest and G. Thomas, to be published.

TABLE I

| Fault Type | Composition of Removed Material | Octahedra-Tetrahedra Share | Shortest A-B Distance | Tetrahedra Tetrahedra Share | Shortest A-A Distance |
|---|---|---|---|---|---|
| Perfect | --- | corners | $d_{113} = .414a_o$ | --- | $d_{111} = .434a_o$ |
| (100) 1/4[110] | $A\ B_2\ O_4$ | faces | $d_{111} = .217a_o$ | corners | $d_{110} = .354a_o$ |
| (100) 1/4[011]1) | --- | faces | $d_{111} = .217a_o$ | --- | $d_{111} = .434a_o$ |
| | | corners | $d_{113} = .414a_o$ | edges | $d_{100} = .250a_o$ |
| (110) 1/4[110] | $A\ B_2\ O_4$ | corners | $d_{113} = .414a_o$ | corners | $d_{110} = .354a_o$ |
| (110) 1/4[1$\bar{1}$0] | --- | faces | $d_{111} = .217a_o$ | --- | $d_{111} = .434a_o$ |
| (110) 1/4[101] | $A\ B\ O_2$ | corners | $d_{113} = .414a_o$ | --- | $d_{111} = .434a_o$ |
| | $B\ O_2$ | faces | $d_{111} = .217a_o$ | edges | $d_{100} = .250a_o$ |
| (111) 1/4[110] | $B_3\ O_4$ | corners | $d_{113} = .414a_o$ | edges | $d_{100} = .250a_o$ |
| | $A_2\ B\ O_4$ | corners | $d_{113} = .414a_o$ | --- | $d_{111} = .434a_o$ |
| | $A\ B_3\ O_4$ | corners | $d_{113} = .414a_o$ | corners | $d_{110} = .354a_o$ |
| | $A\ B\ O_4$ | faces | $d_{111} = .217a_o$ | corners | $d_{110} = .354a_o$ |
| (111) 1/4[1$\bar{1}$0] | --- | faces | $d_{111} = .217a_o$ | --- | $d_{111} = .434a_o$ |
| | ---2) | faces | $d_{111} = .217a_o$ | edges | $d_{100} = .250a_o$ |

1) The configuration of the ions depends on the exact position of the fault plane and the direction of shear.

2) In case the fault plane breaks up a "mixed" cation layer.

TABLE II

(111) Stacking of Ions in the Spinel Structure [13]

| Level | Occupied Position | Composition | |
|---|---|---|---|
| 14 | a 1,2,3,4 | $O_4$ | |
| 13 | --- | --- | $B_3O_4$ (kagomé) |
| 12 | c 2,3,4 | $B_3$ | |
| 11 | --- | --- | |
| 10 | b 1,2,3,4 | $O_4$ | |
| 9 | c 1 | A | $A_2BO_4$ (mixed) |
| 8 | a 1 | B | |
| 7 | b 1 | A | |
| 6 | c 1,2,3,4 | $O_4$ | $A\ B_3\ O_4$ |
| 5 | --- | --- | |
| 4 | b 2,3,4 | $B_3$ | |
| 3 | --- | --- | |
| 2 | a 1,2,3,4 | $O_4$ | $A\ B\ O_4$ |
| 1 | b 1 | A | |
| 0 | c 1 | B | |
| -1 | a 1 | A | |

Table III. Coordinates of octahedral sites.

| No. | x | y | z |
|---|---|---|---|
| 1 | 0.625 | 0.625 | 0.625 |
| 2 | 0.125 | 0.875 | 0.375 |
| 3 | 0.375 | 0.125 | 0.875 |
| 4 | 0.875 | 0.375 | 0.125 |
| 5 | 0.125 | 0.375 | 0.875 |
| 6 | 0.875 | 0.125 | 0.375 |
| 7 | 0.375 | 0.875 | 0.125 |
| 8 | 0.375 | 0.625 | 0.375 |
| 9 | 0.375 | 0.375 | 0.625 |
| 10 | 0.625 | 0.375 | 0.375 |
| 11 | 0.625 | 0.125 | 0.125 |
| 12 | 0.125 | 0.625 | 0.125 |
| 13 | 0.125 | 0.125 | 0.625 |
| 14 | 0.875 | 0.875 | 0.625 |
| 15 | 0.625 | 0.875 | 0.875 |
| 16 | 0.875 | 0.625 | 0.875 |

Table IV. Atomic coordinates of the eight ordered arrangements.

| Symbol | Arrangement | Atomic Coordinates* |
|---|---|---|
| 1L | $P4_332$ | Li: 1, 2, 3, 4** |
| 2L | $P4_332 + \frac{1}{2}[110]^{\dagger}$ | Li: 7, 10, 13, 16 |
| 3L | $P4_332 + \frac{1}{2}[101]$ | Li: 6, 9, 12, 15 |
| 4L | $P4_332 + \frac{1}{2}[011]$ | Li: 5, 8, 11, 14 |
| 1R | $P4_132$ | Li: 1, 5, 6, 7 |
| 2R | $P4_132 + \frac{1}{2}[110]$ | Li: 4, 8, 13, 15 |
| 3R | $P4_132 + \frac{1}{2}[101]$ | Li: 3, 10, 12, 14 |
| 4R | $P4_132 + \frac{1}{2}[011]$ | Li: 4, 9, 11, 16 |

*The octahedral sites not occupied by lithium are occupied by the iron ions. Only the position of the lithium ions are given. The position of the oxygen ions and tetrahedral ions are the same for all the ordered arrangements.

**These numbers refer to the numbers of the octahedral sites as given in Table III.

†$P4_332 + \frac{1}{2}[110]$ means that this arrangement is derived from the "basic" $P4_332$ arrangement by giving the Li ions a displacement over a vector $\frac{1}{2}[110]$.

Table V. Classification of Boundaries.*

| $T_1$ | $T_2$ | $T_3$ | I | $I+T_1$ | $I+T_2$ | $I+T_3$ |
|---|---|---|---|---|---|---|
| LL-2L | 1L-3L | 1L-4L | 1L-1R | 1L-2R | 1L-3R | 1L-4R |
| 3L-4L | 2L-4L | 2L-3L | 2L-2R | 2L-1R | 2L-4R | 2L-3R |
| 1R-2R | 1R-3R | 1R-4R | 3L-3R | 3L-4R | 3L-1R | 3L-2R |
| 3R-4R | 3R-4R | 2R-3R | 4L-4R | 4L-4R | 4L-2R | 4L-1R |

*Symbols used in this table are explained in Table IV and in Fig. 10.

Table VI. Values of the phase angle $\alpha$.

| C | $T_1$ | $T_2$ | $T_3$ | I | $I+T_1$ | $I+T_2$ | $I+T_3$ |
|---|---|---|---|---|---|---|---|
| 110 | 0 | $\pi$ | $\pi$ | 0 | 0 | $\pi$ | $\pi$ |
| $1\bar{1}0$ | 0 | $\pi$ | $\pi$ | $\pi$ | $\pi$ | 0 | 0 |
| 101 | $\pi$ | 0 | $\pi$ | 0 | $\pi$ | 0 | $\pi$ |
| $10\bar{1}$ | $\pi$ | 0 | $\pi$ | $\pi$ | 0 | $\pi$ | 0 |
| 011 | $\pi$ | $\pi$ | 0 | 0 | $\pi$ | $\pi$ | 0 |
| $01\bar{1}$ | $\pi$ | $\pi$ | 0 | $\pi$ | 0 | 0 | $\pi$ |
| 112 | 0 | $\pi$ | $\pi$ | 0 | 0 | $\pi$ | $\pi$ |
| $\bar{1}12$ | 0 | $\pi$ | $\pi$ | $\pi$ | $\pi$ | 0 | 0 |
| $1\bar{1}2$ | 0 | $\pi$ | $\pi$ | $\pi$ | $\pi$ | 0 | 0 |
| $\bar{1}\bar{1}2$ | 0 | $\pi$ | $\pi$ | 0 | 0 | $\pi$ | $\pi$ |
| 211 | $\pi$ | $\pi$ | 0 | 0 | $\pi$ | $\pi$ | 0 |
| $21\bar{1}$ | $\pi$ | $\pi$ | 0 | $\pi$ | 0 | 0 | $\pi$ |
| $2\bar{1}1$ | $\pi$ | $\pi$ | 0 | $\pi$ | 0 | 0 | $\pi$ |
| $2\bar{1}\bar{1}$ | $\pi$ | $\pi$ | 0 | 0 | $\pi$ | $\pi$ | 0 |
| 121 | $\pi$ | 0 | $\pi$ | 0 | $\pi$ | 0 | $\pi$ |
| $12\bar{1}$ | $\pi$ | 0 | $\pi$ | $\pi$ | 0 | $\pi$ | 0 |
| $\bar{1}21$ | $\pi$ | 0 | $\pi$ | $\pi$ | 0 | $\pi$ | 0 |
| $\bar{1}2\bar{1}$ | $\pi$ | 0 | $\pi$ | 0 | $\pi$ | 0 | $\pi$ |
| $\bar{1}20$ | $\pi$ | $\pi$ | 0 | $\pi/2$ | $-\pi/2$ | $-\pi/2$ | $\pi/2$ |
| 120 | $\pi$ | $\pi$ | 0 | $-\pi/2$ | $\pi/2$ | $\pi/2$ | $-\pi/2$ |
| 210 | $\pi$ | 0 | $\pi$ | $\pi/2$ | $-\pi/2$ | $\pi/2$ | $-\pi/2$ |
| $\bar{2}10$ | $\pi$ | 0 | $\pi$ | $\pi/2$ | $-\pi/2$ | $\pi/2$ | $-\pi/2$ |
| 021 | 0 | $\pi$ | $\pi$ | $\pi/2$ | $\pi/2$ | $-\pi/2$ | $-\pi/2$ |
| $0\bar{2}1$ | 0 | $\pi$ | $\pi$ | $\pi/2$ | $\pi/2$ | $-\pi/2$ | $-\pi/2$ |
| 012 | $\pi$ | 0 | $\pi$ | $-\pi/2$ | $\pi/2$ | $-\pi/2$ | $\pi/2$ |
| $0\bar{1}2$ | $\pi$ | 0 | $\pi$ | $\pi/2$ | $-\pi/2$ | $\pi/2$ | $-\pi/2$ |
| 102 | $\pi$ | $\pi$ | 0 | $\pi/2$ | $-\pi/2$ | $-\pi/2$ | $\pi/2$ |
| $\bar{1}02$ | $\pi$ | $\pi$ | 0 | $-\pi/2$ | $\pi/2$ | $\pi/2$ | $-\pi/2$ |
| 201 | 0 | $\pi$ | $\pi$ | $-\pi/2$ | $-\pi/2$ | $\pi/2$ | $\pi/2$ |
| $20\bar{1}$ | 0 | $\pi$ | $\pi$ | $\pi/2$ | $\pi/2$ | $-\pi/2$ | $-\pi/2$ |

Table VII. Analysis of Fig. 11.

| Boundary* | $g=\bar{1}10$ | $g=0\bar{1}1$ | $g=\bar{1}01$ | Type |
|---|---|---|---|---|
| a | NC** | NC | C† | $I+T_2$ |
| b | NC | C | C | $T_1$ |
| c | NC | C | NC | $I+T_3$ |
| d | C | NC | C | $T_3$ |
| e | NC | C | NC | $I+T_3$ |
| f | C | NC | NC | $I+T_1$ |
| g | NC | C | C | $T_1$ |
| h | C | NC | NC | $I+T_1$ |
| i | C | C | NC | $T_2$ |
| j | C | C | NC | $T_2$ |
| k | C | NC | NC | $I+T_1$ |
| ℓ | NC | C | NC | $I+T_3$ |

*The boundaries are labelled in Fig. 11a.

**NC: boundary not in contrast.

†C: boundary in contrast.

FIGURE CAPTIONS

Fig. 1. Typical arrangement of cation stacking faults in lithium ferrite. Notice at A, the disappearance of fringes at overlapping faults. At B three faults meet along a line. One fault is seen edge on. In the region where the other two overlap, fringes run parallel with the line of intersection. This arrangement of faults corresponds with the one in Fig. 8b. At C there is an arrangement corresponding with Fig. 8a (one fault seen edge-on).

Fig. 2. Three faults meeting at a junction of fully ordered lithium ferrite. Only spinel reflections have been used in these photographs. These diffraction experiments allow one to determine the displacement vector of these faults and the Burgers vector of the dislocation confining fault A.

Fig. 3. Projection of an ideal spinel structure on the (001) plane. Oxygen ions have been omitted. A fault on (100) was introduced into the structure, with the displacement vector at 45° to the fault plane. For some ions the coordination polyhedra are shown. Octahedra and tetrahedra project as squares. In the perfect structure, octahedra and tetrahedra share corners, while across the fault plane they share faces (hatched area). Across the fault plane tetrahedra share corners, whereas in the perfect structure they do not touch.

Fig. 4. Only three layers of ions are shown here. The shear necessary for a {001} 1/4⟨110⟩ type fault are shown. The plane of the fault is parallel with the plane of the paper, and is located between the layer at 0 and the layer at 1. Coordination tetrahedra

project as the smaller squares, octahedra as the large one. After shear in the $[\bar{1}\bar{1}0]$ direction, tetrahedra share an edge (indicated by -.-.-) at C. After shear in the $[1\bar{1}0]$ direction a tetrahedron shares a face (hatched) with the octahedron at A and also with the octahedron at B (not shown).

Fig. 5. Same type of projection as in Fig. 3. A fault on (110) was introduced with the displacement vector in the plane of the fault. Across the fault plane octahedra and tetrahedra share faces.

Fig. 6. Same type of projection as in Fig. 3. A fault on (110) was introduced with the displacement vector orthogonal to the fault plane. Notice that octahedra and tetrahedra are not displaced relative to one another. Tetrahedra, however, share corners across the fault plane.

Fig. 7. Projection of an ideal spinel structure on the (110) plane. A two dimensional unit cell is shown, which can be used to determine the composition in successive (110) planes. A $(1\bar{1}0)$ $1/4[1\bar{1}0]$ fault has been introduced. Across the fault plane tetrahedral ions have an oxygen ion in common as a nearest neighbor.

Fig. 8. Two possible modes by which a {110} 1/4⟨110⟩ fault can change fault planes. (a) By leaving a dislocation at the junction. (b) When the three faults meet at a junction a dislocation is not necessary.

Fig. 9. Projection of the octahedral sites on the (100) plane for the two enantiomorphs. The unit cell indicated is the conventional one for the $P4_332$ spacegroup. It is indicated how the octahedral sites are aligned in ⟨011⟩ directions with one Li ion followed by three Fe ions.

Fig. 10. Schematic representation of the seven different boundaries in ordered $LiFe_5O_8$. The labels of the ordered arrangements are explained in Table II.

Fig. 11. An identical area of an ordered crystal photographed under five different diffraction conditions. The operating reflections in (a), (b), (c) and (d) are indicated by vectors. The diffraction pattern corresponding to (e) and (f) is shown in (g) (BF: bright field; DF: dark field with reflection used indicated). The specimen was annealed at 850°C and furnace cooled.

Fig. 12. Bright field (a) and two dark fields (b,c) showing that a few fairly strong reflections off the operating row are sufficient to produce strong differences in contrast between enantiomorphic domain (e.g., at A and B). Across translation boundaries there is no difference in background intensity (e.g., at C and D). The specimen was annealed at 850°C and furnace cooled.

Fig. 13. Domains in a crystal in the as received condition. The domain size is of the order of 5μ.

Fig. 14. This specimen was annealed at 950°C for 30 min, water quenched, then annealed at 650°C for 100 min. The domain size is of the order of 0.2μ.

Fig. 15. Fault A in this micrograph is an example of a 1/4⟨112⟩ type fault in ordered lithium ferrite. The fault plane is $(0\bar{1}1)$ and $R = \pm 1/4[211]$. A $\pm 1/4[0\bar{1}1]$ displacement vector would have been out of contrast in (a) ($g \cdot R = 0$) and in contrast in (b) which is contrary to the observations.

Fig. 16. Three stacking faults forming a triple junction in ordered lithium ferrite. The same area was photographed under four different diffraction conditions, characterized by the g vectors in the figures.

Fig. 17. Figure 17a was taken under the conditions shown in Fig. 17b. Figure 17c was taken under the diffraction conditions indicated in the figure.

Fig. 18. Contrast conditions are shown for a translation fault (a), a (101) fault (b) and 1/4[101] partials (c). Weak $\pi$ contrast occurs in (b) due to the influence of the superlattice reflections in the systematic set. (c) shows the advantage of using high resolution images in $n\bar{g}$ ($n = 6$) in which the two partials are well resolved.

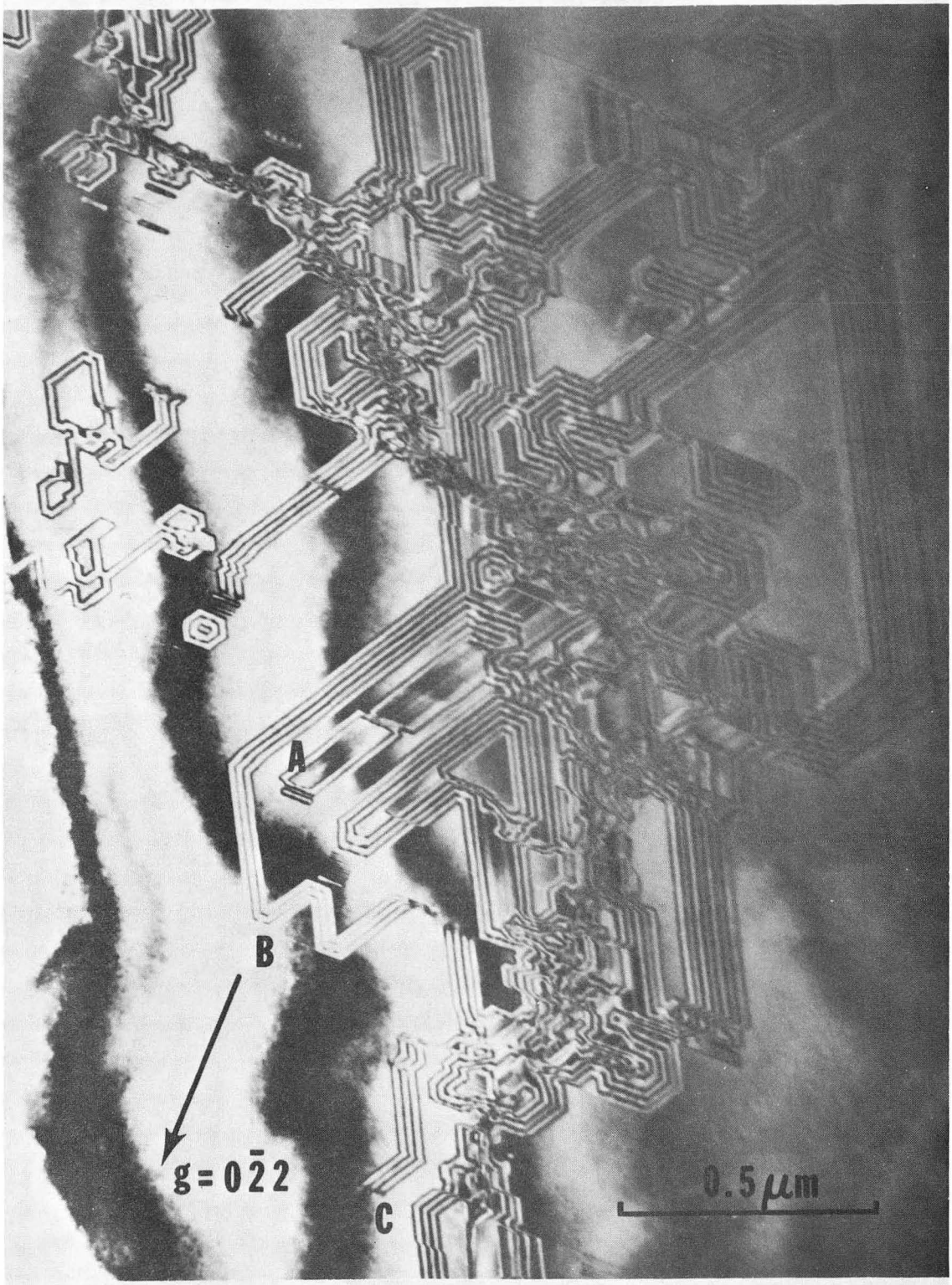


XBB 742-813

Fig. 1.

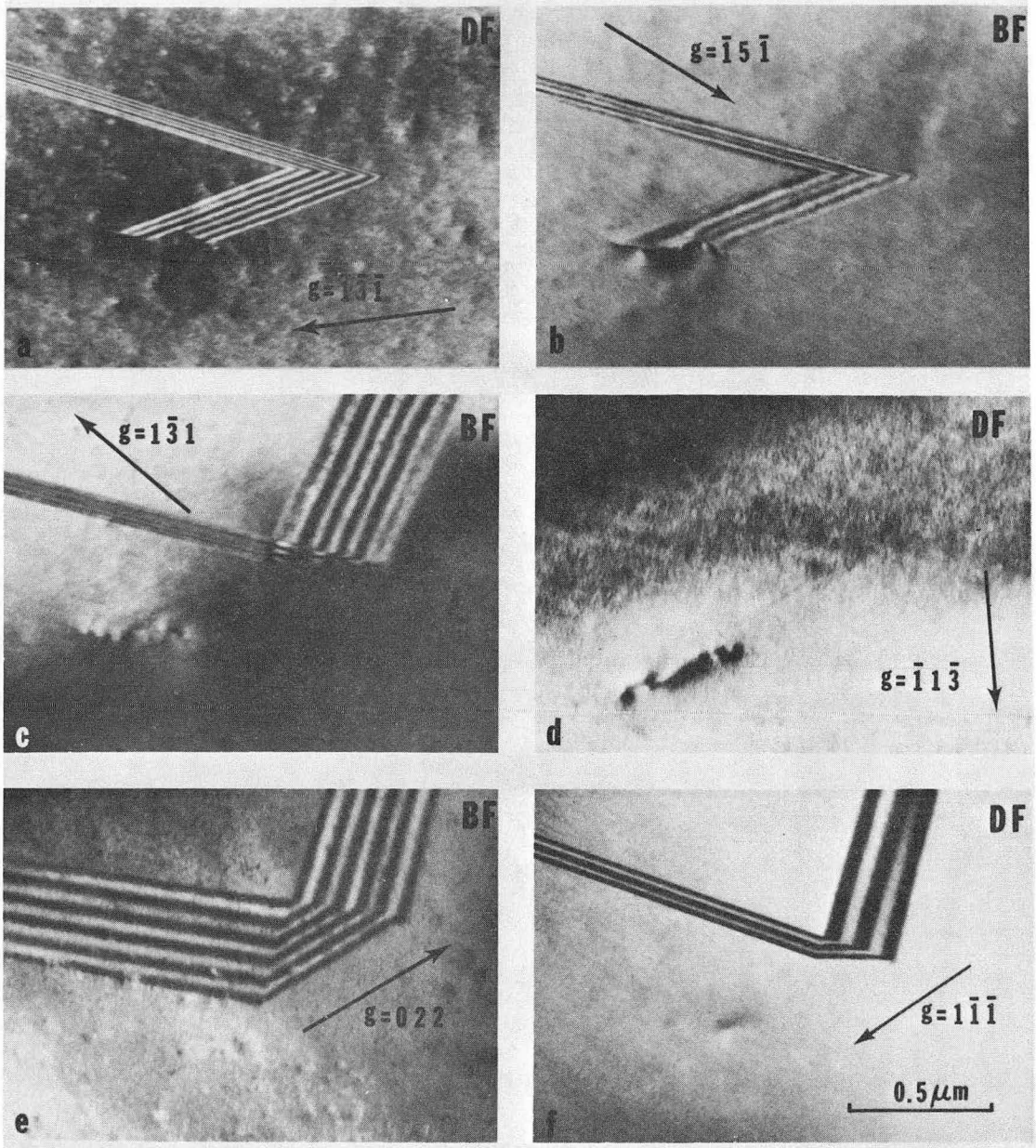


XBB 742-814

Fig. 2.

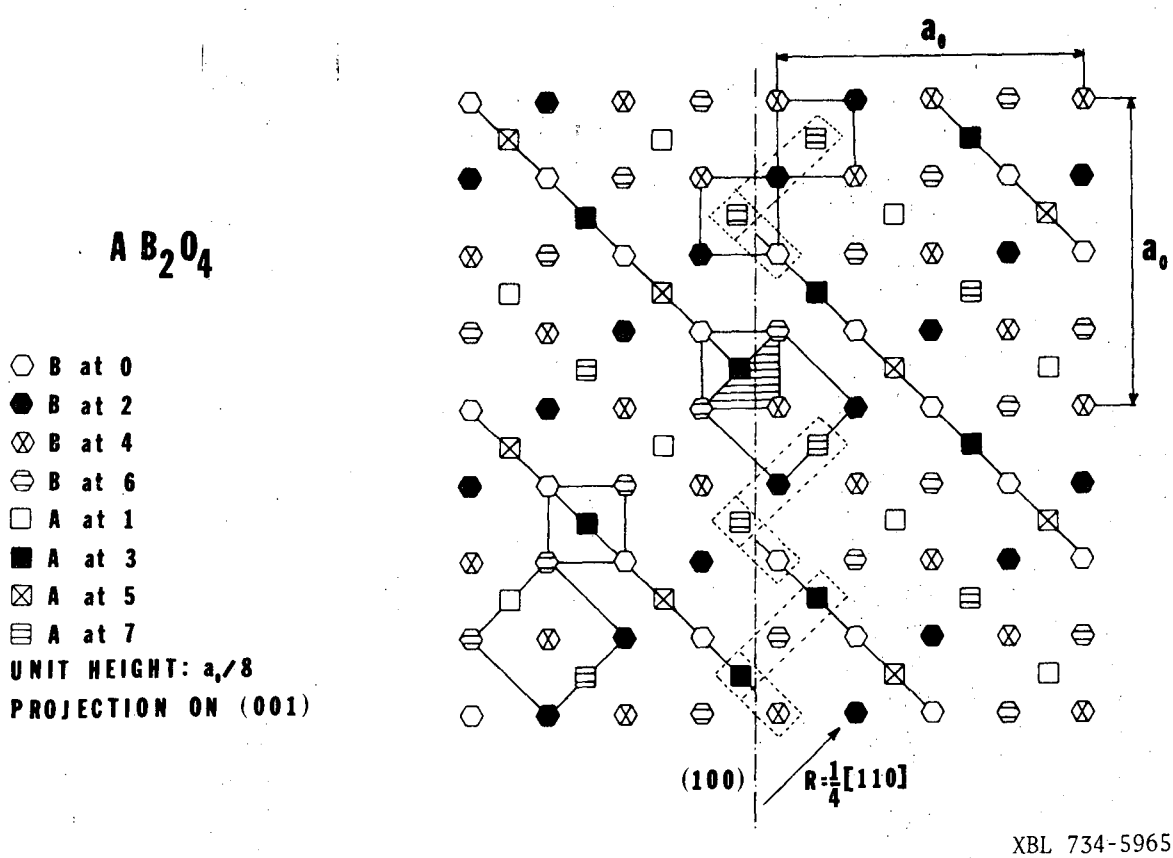
$AB_2O_4$
B at 0
B at 2
B at 4
B at 6
A at 1
A at 3
A at 5
A at 7
UNIT HEIGHT: $a_0/8$
PROJECTION ON (001)
$a_0$
$a_0$
(100)
$R=\frac{1}{4}[110]$
XBL 734-5965

Fig. 3.

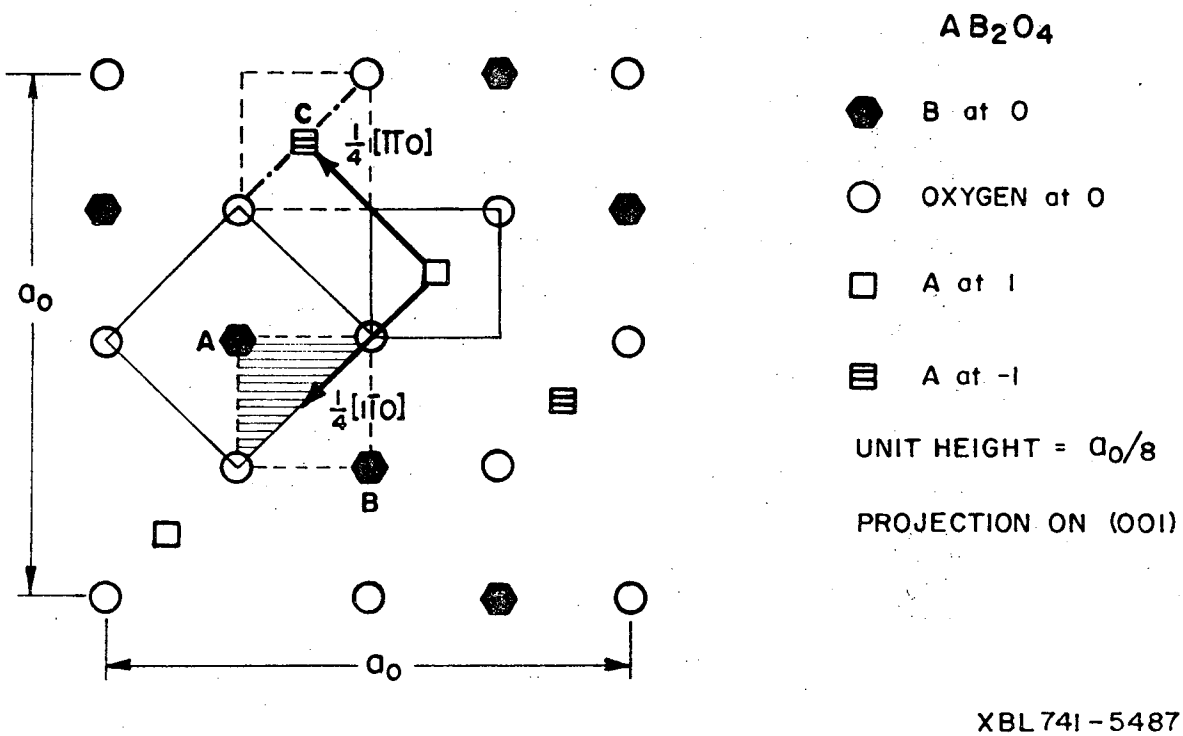
$AB_2O_4$
B at 0
OXYGEN at 0
A at 1
A at -1
UNIT HEIGHT = $a_0/8$
PROJECTION ON (001)
C
$\frac{1}{4}[\bar{1}\bar{1}0]$
A
$\frac{1}{4}[1\bar{1}0]$
B
$a_0$
$a_0$
XBL 741-5487

Fig. 4.

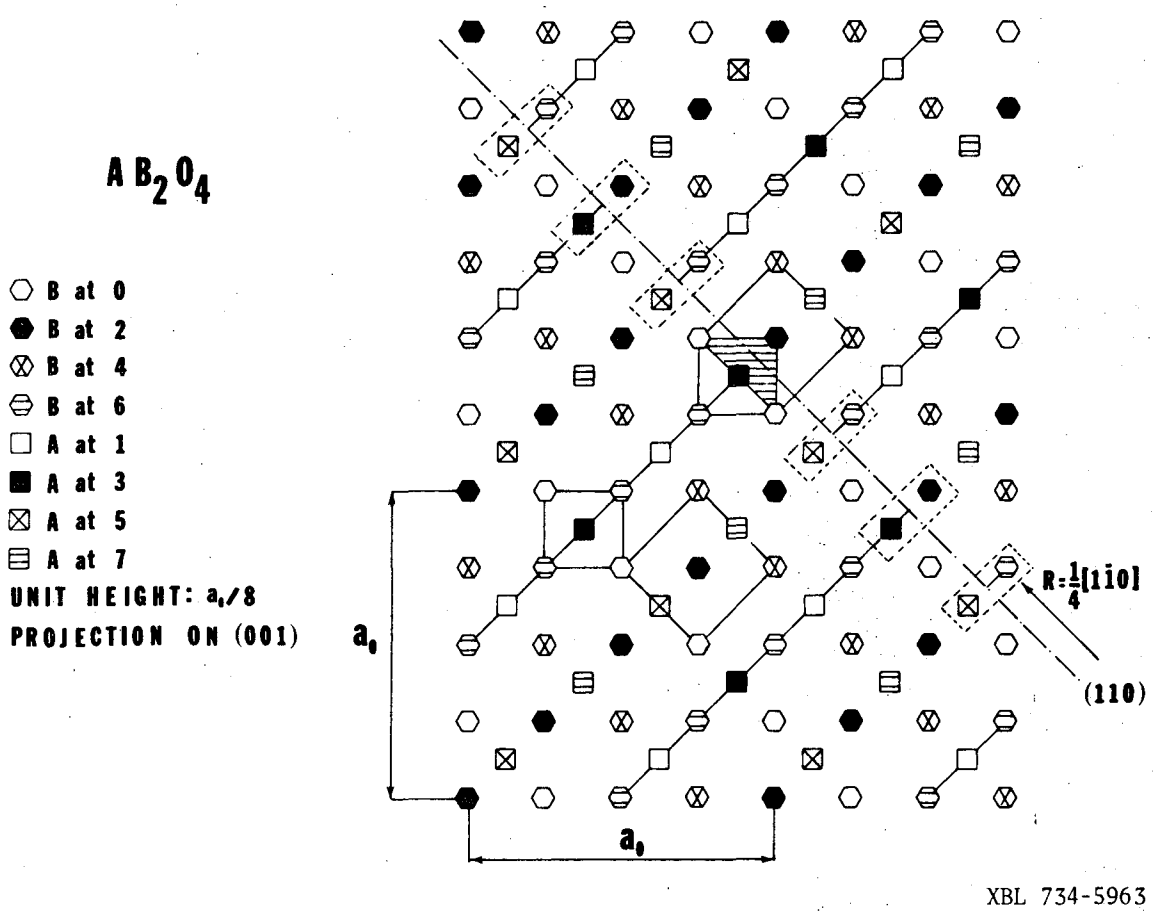
$AB_2O_4$
B at 0
B at 2
B at 4
B at 6
A at 1
A at 3
A at 5
A at 7
UNIT HEIGHT: $a_0/8$
PROJECTION ON (001)
$a_0$
$a_0$
$R=\frac{1}{4}[1\bar{1}0]$
(110)
XBL 734-5963

Fig. 5.

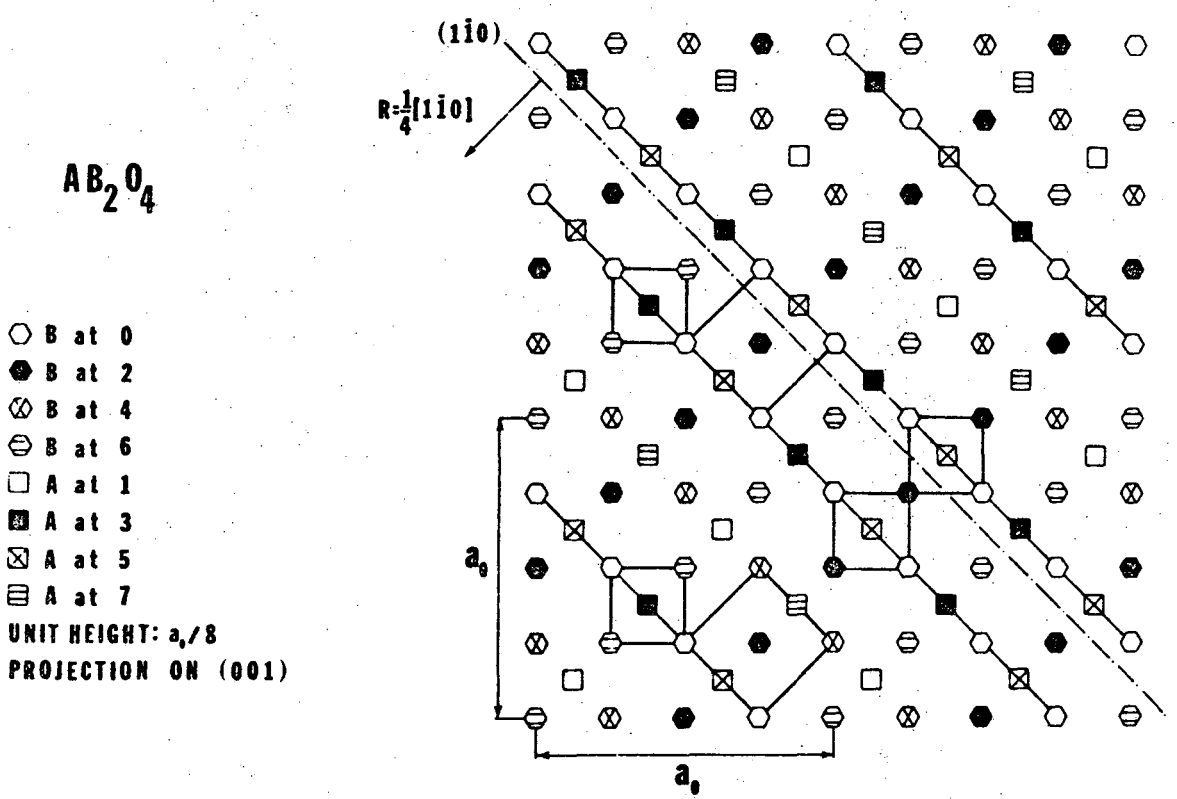


XBL 734-5964A

Fig. 6.

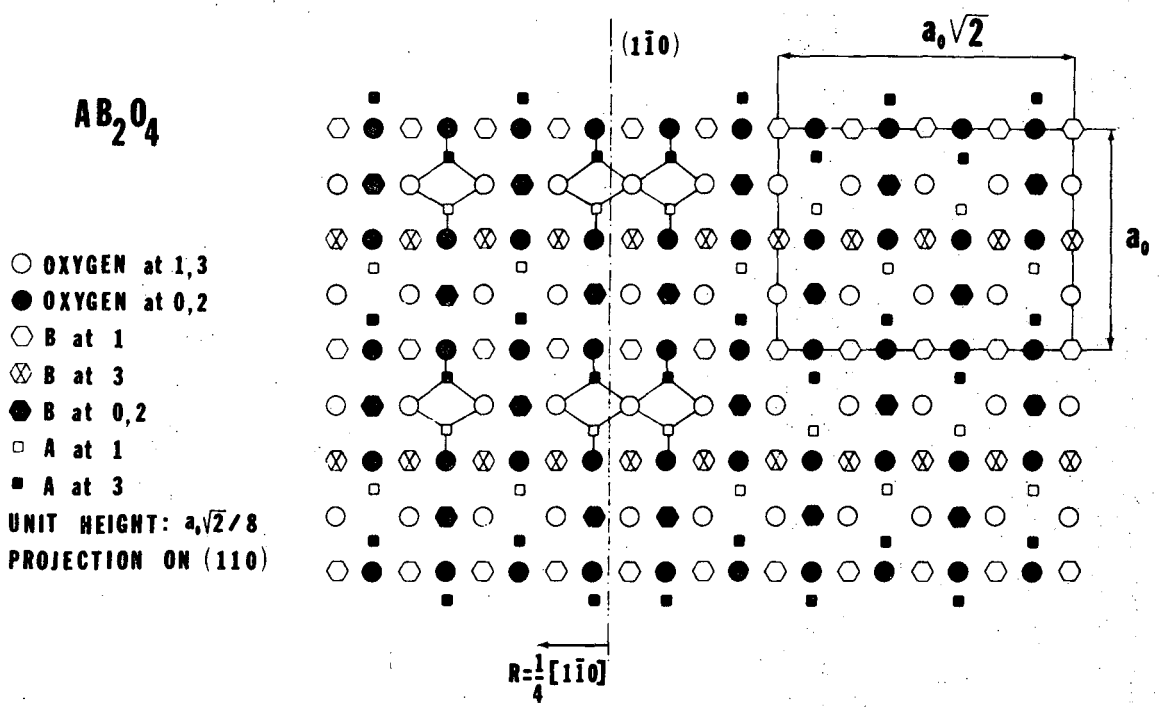


XBL 734-5962A

Fig. 7.

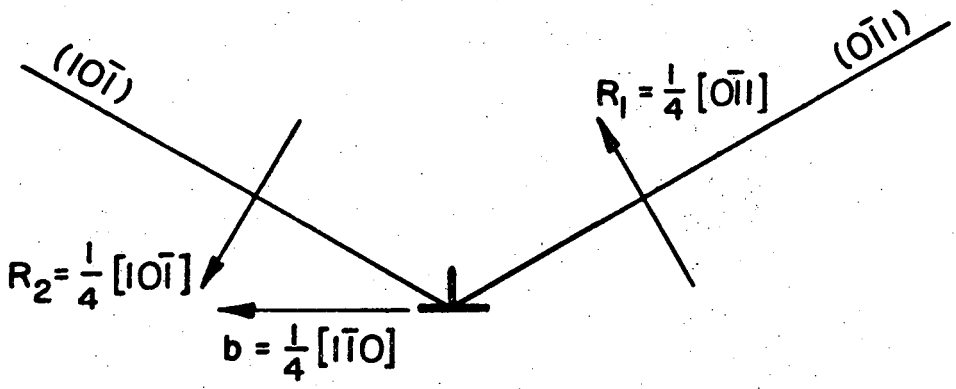


(a)

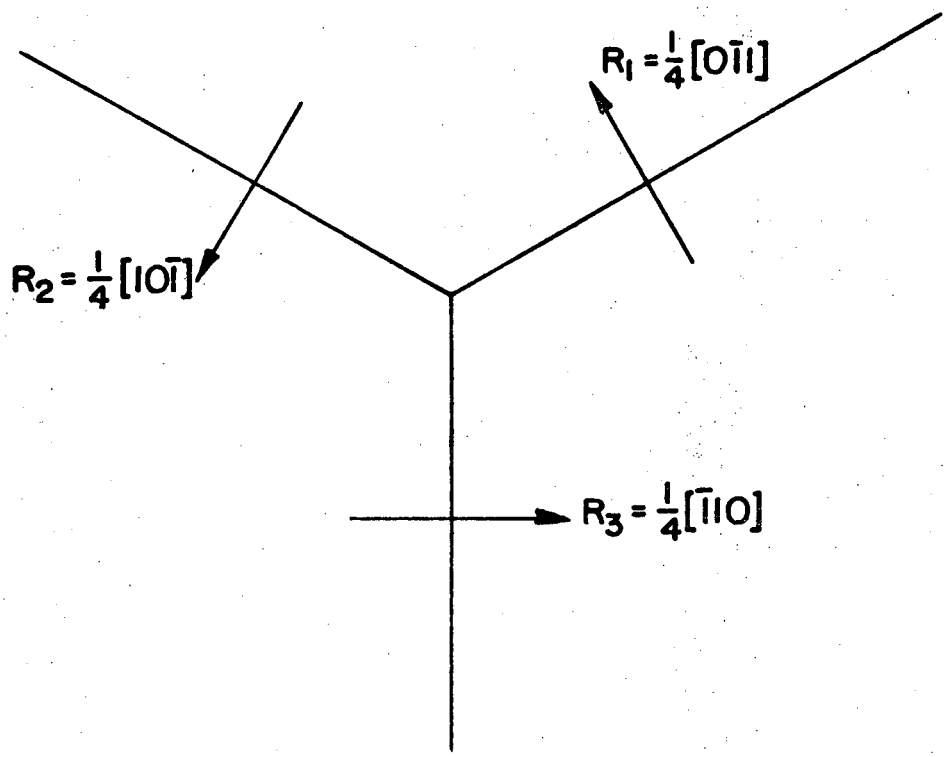


(b)

XBL 7312-7136

Fig. 8.

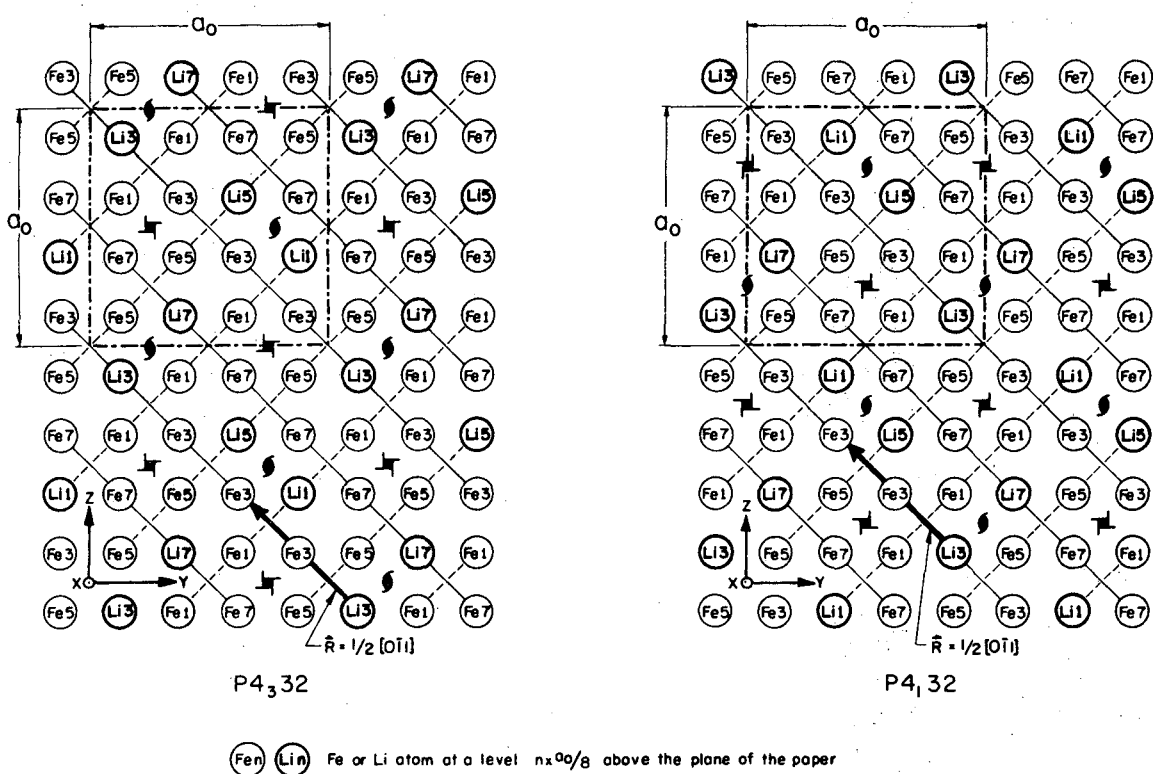
$a_0$
$a_0$
Z
X
Y
$\hat{R} = 1/2\,[0\bar{1}1]$
$P4_3 32$
$P4_1 32$
Fen Lin Fe or Li atom at a level $n \times a_0/8$ above the plane of the paper
XBL745-6281

Fig. 9.

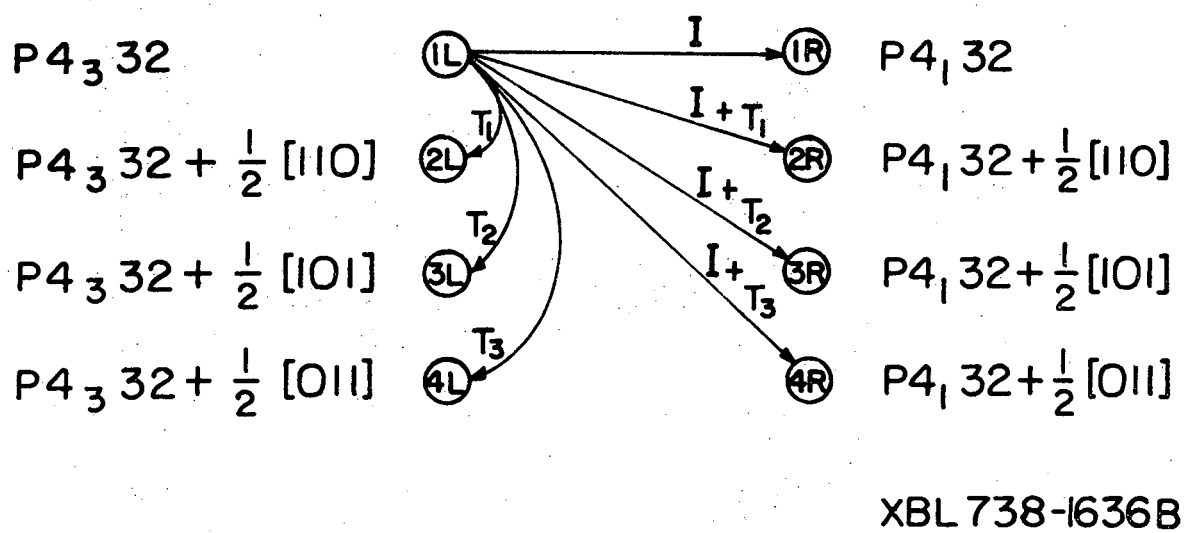
P4₃32
P4₃32 + ½[110]
P4₃32 + ½[101]
P4₃32 + ½[011]
1L
2L
3L
4L
1R
2R
3R
4R
I
I + T₁
I + T₂
I + T₃
T₁
T₂
T₃
P4₁32
P4₁32 + ½[110]
P4₁32 + ½[101]
P4₁32 + ½[011]
XBL 738-1636B

Fig. 10.

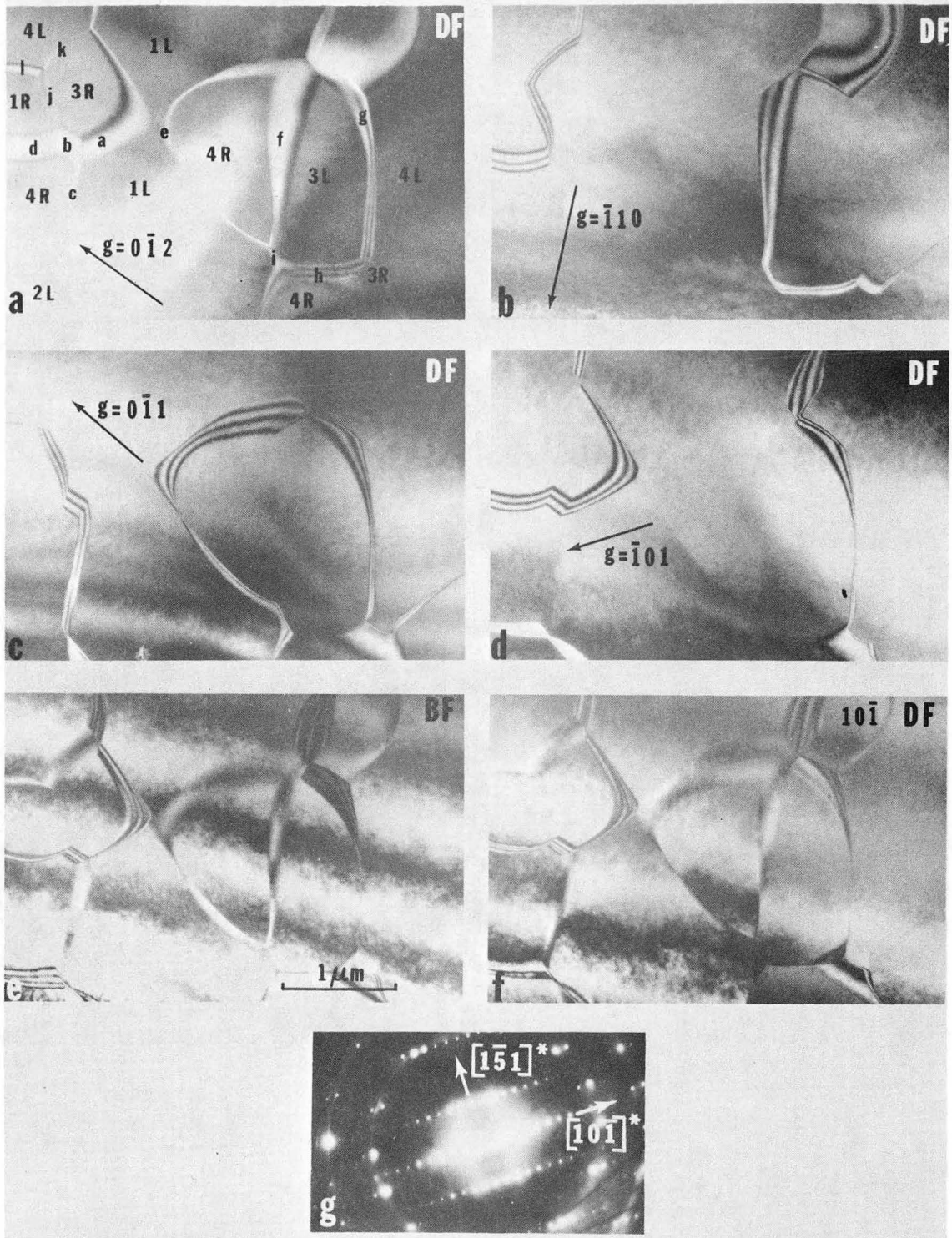


XBB 743-1710

Fig. 11.

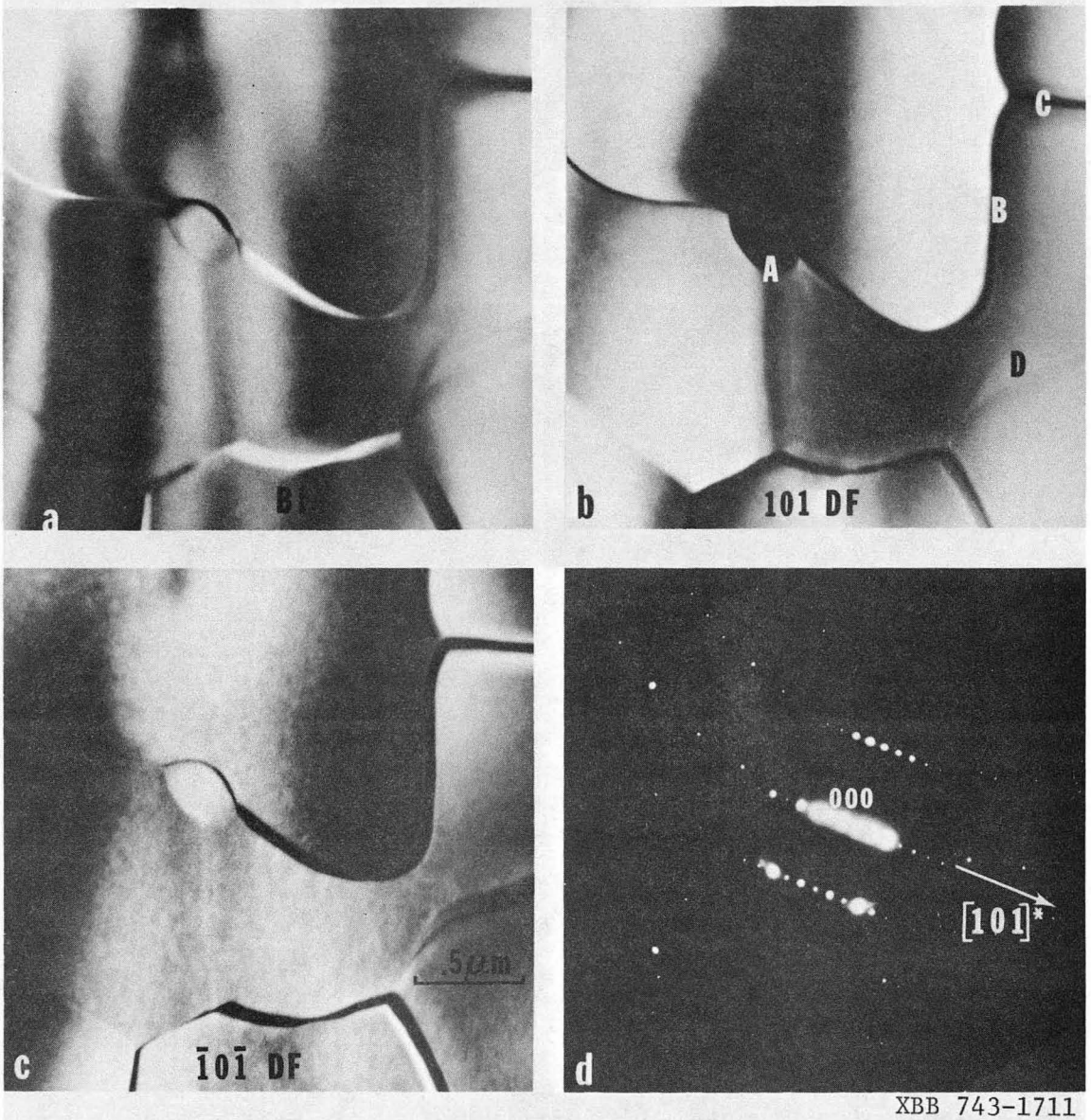


XBB 743-1711

Fig. 12.

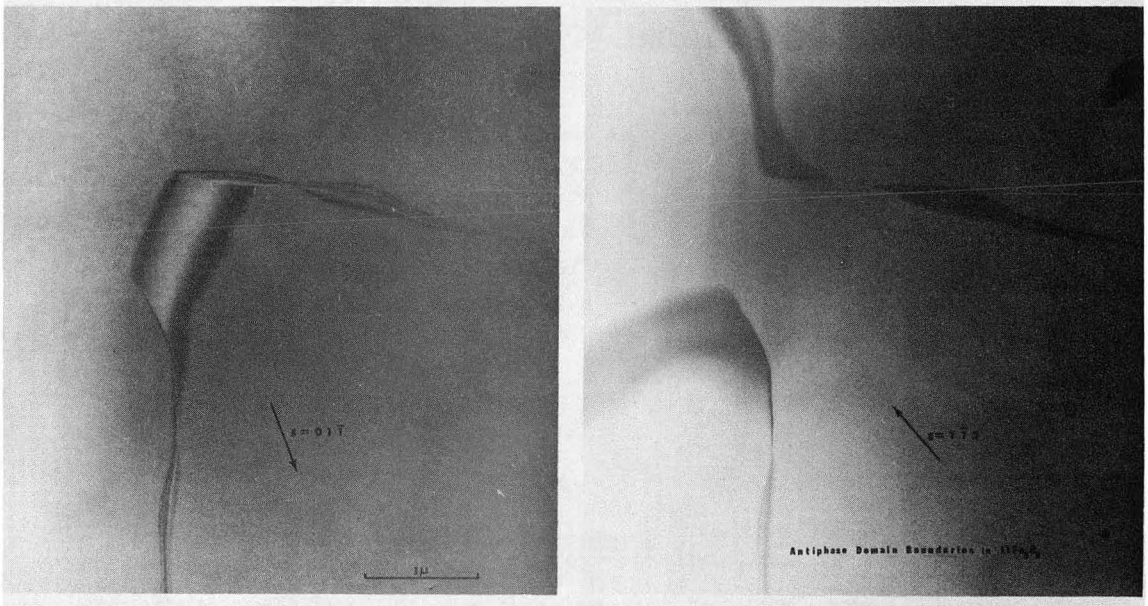


XBB 711-4741

Fig. 13.

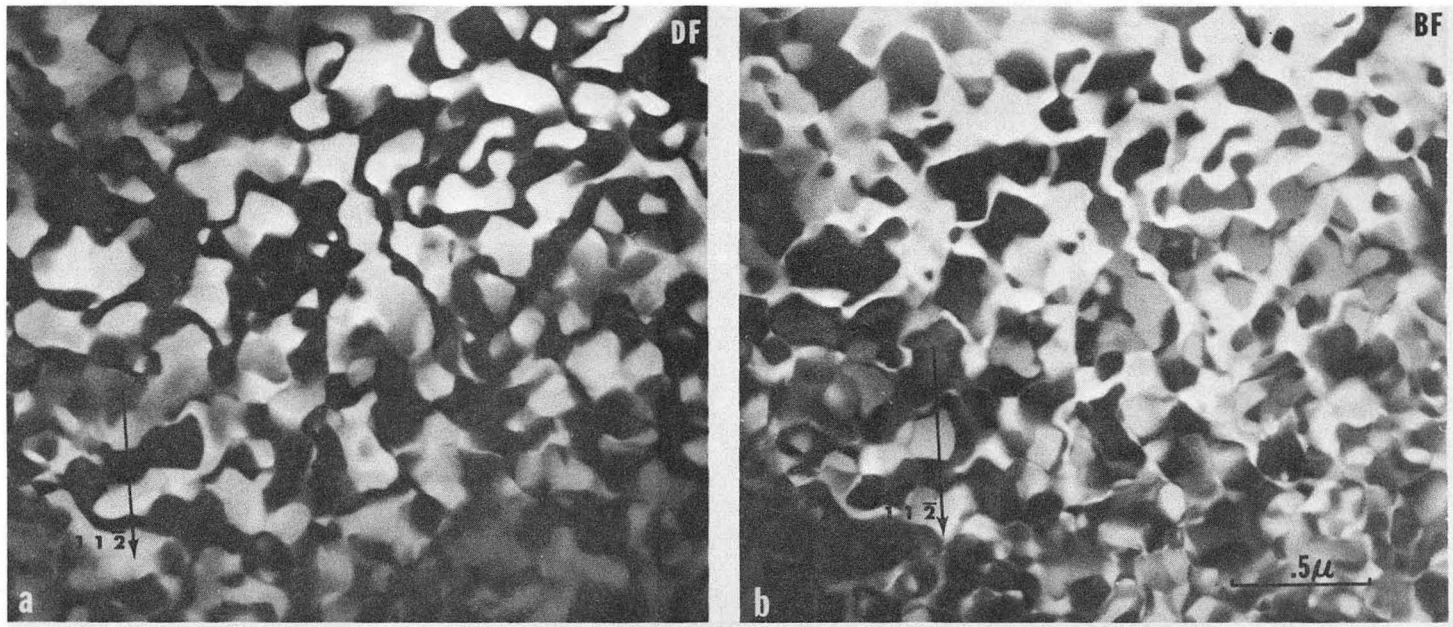


XBB 743-2816

Fig. 14.

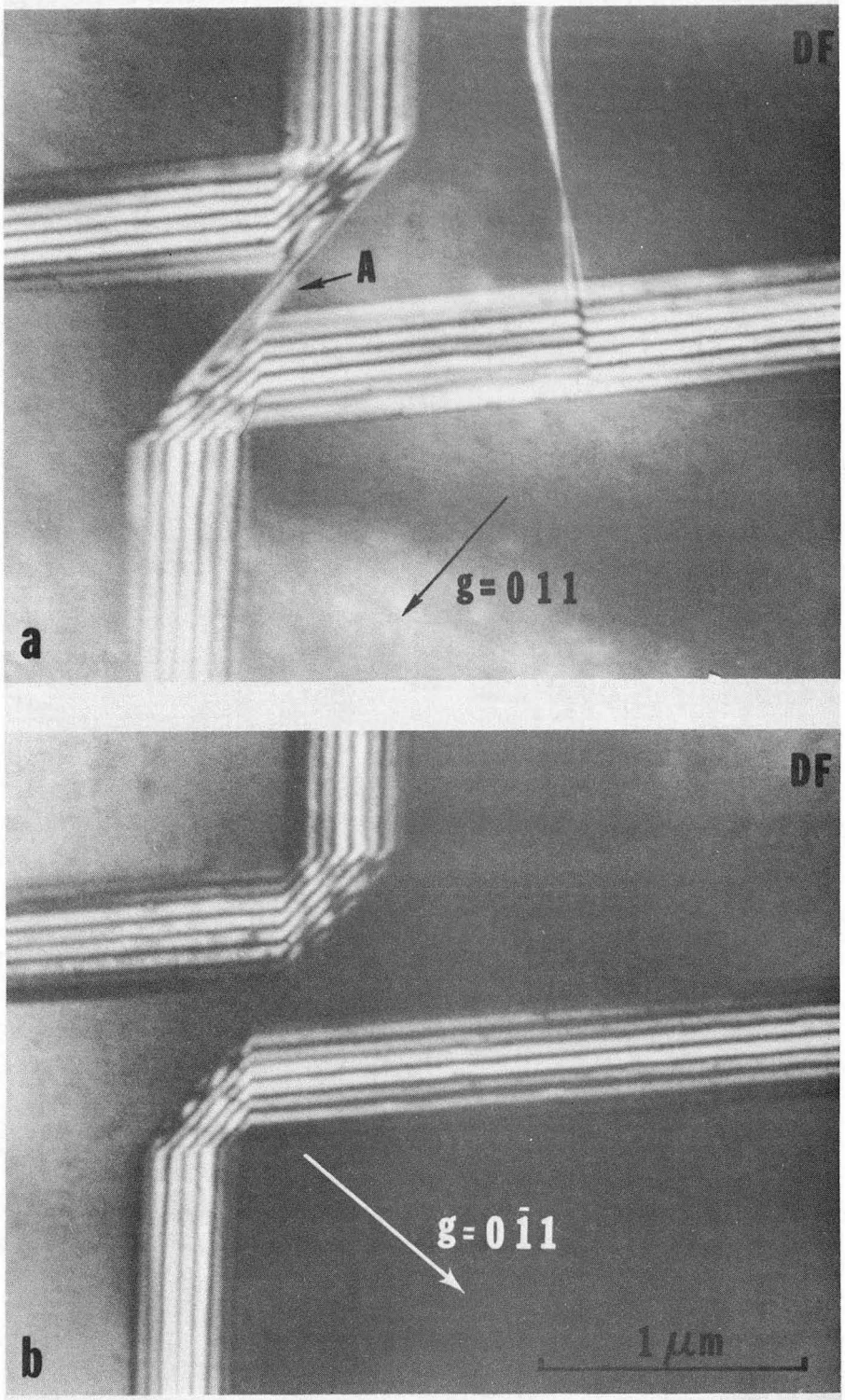


XBB 747-4793

Fig. 15.

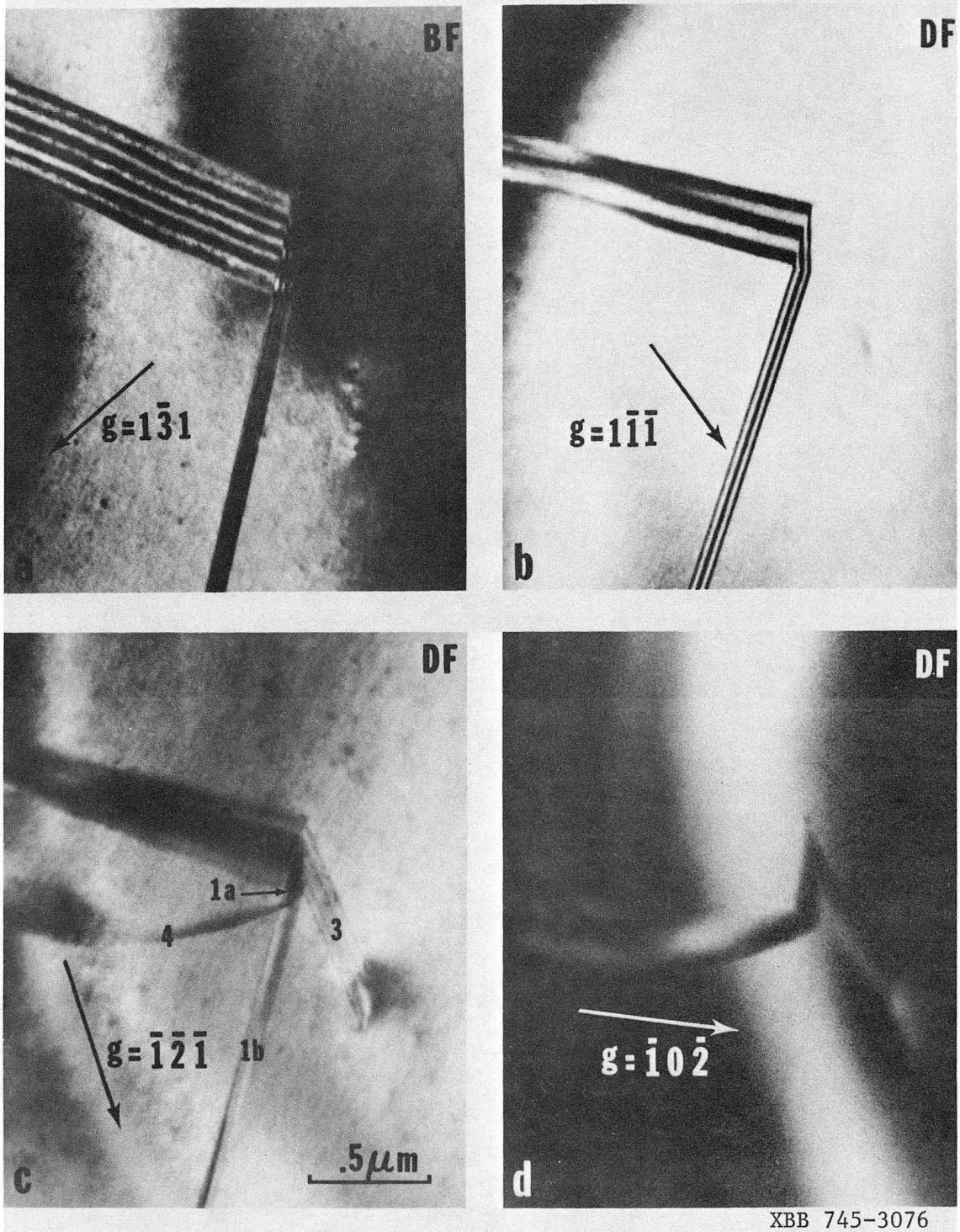


XBB 745-3076

Fig. 16.

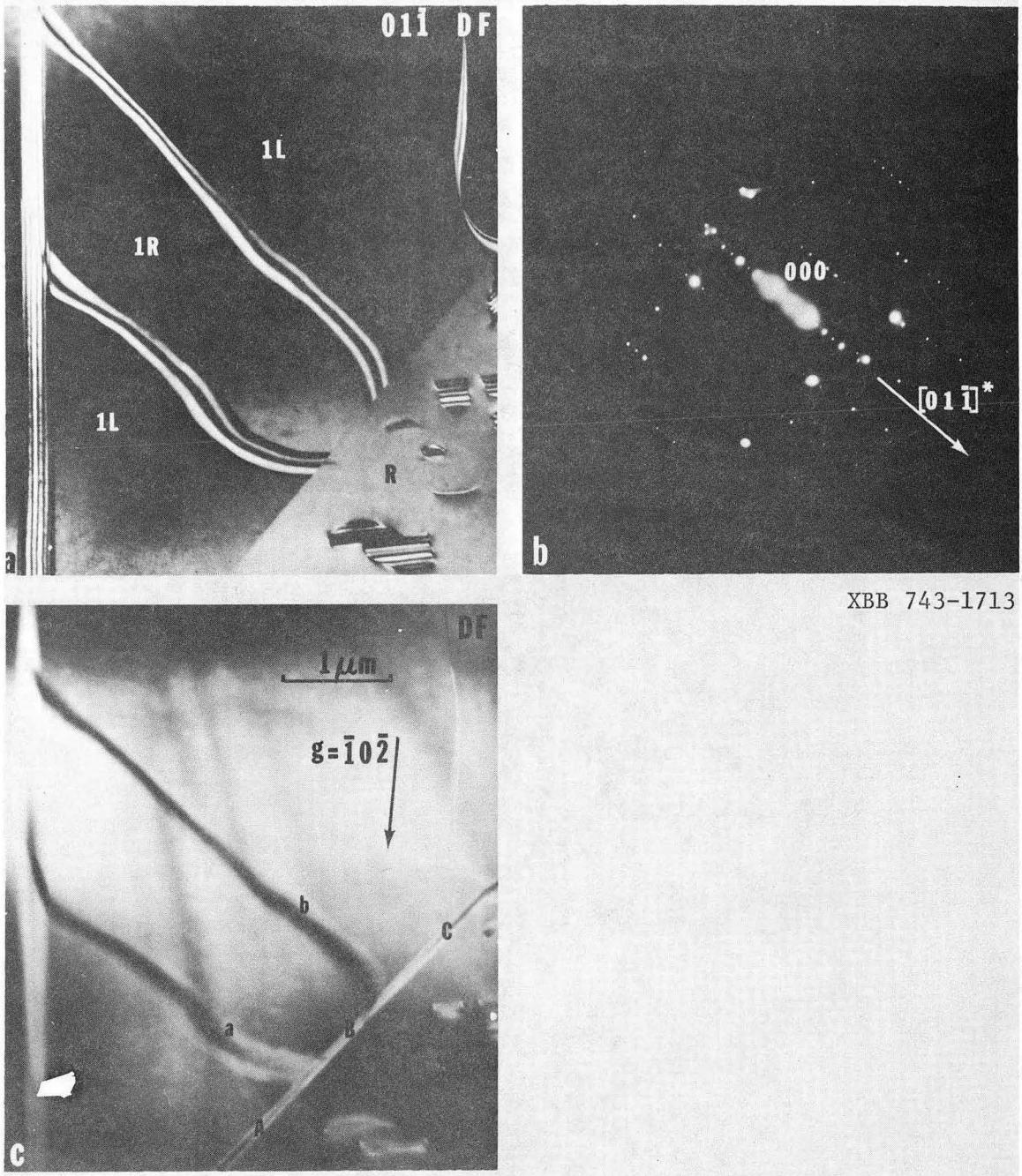


XBB 743-1713

Fig. 17.

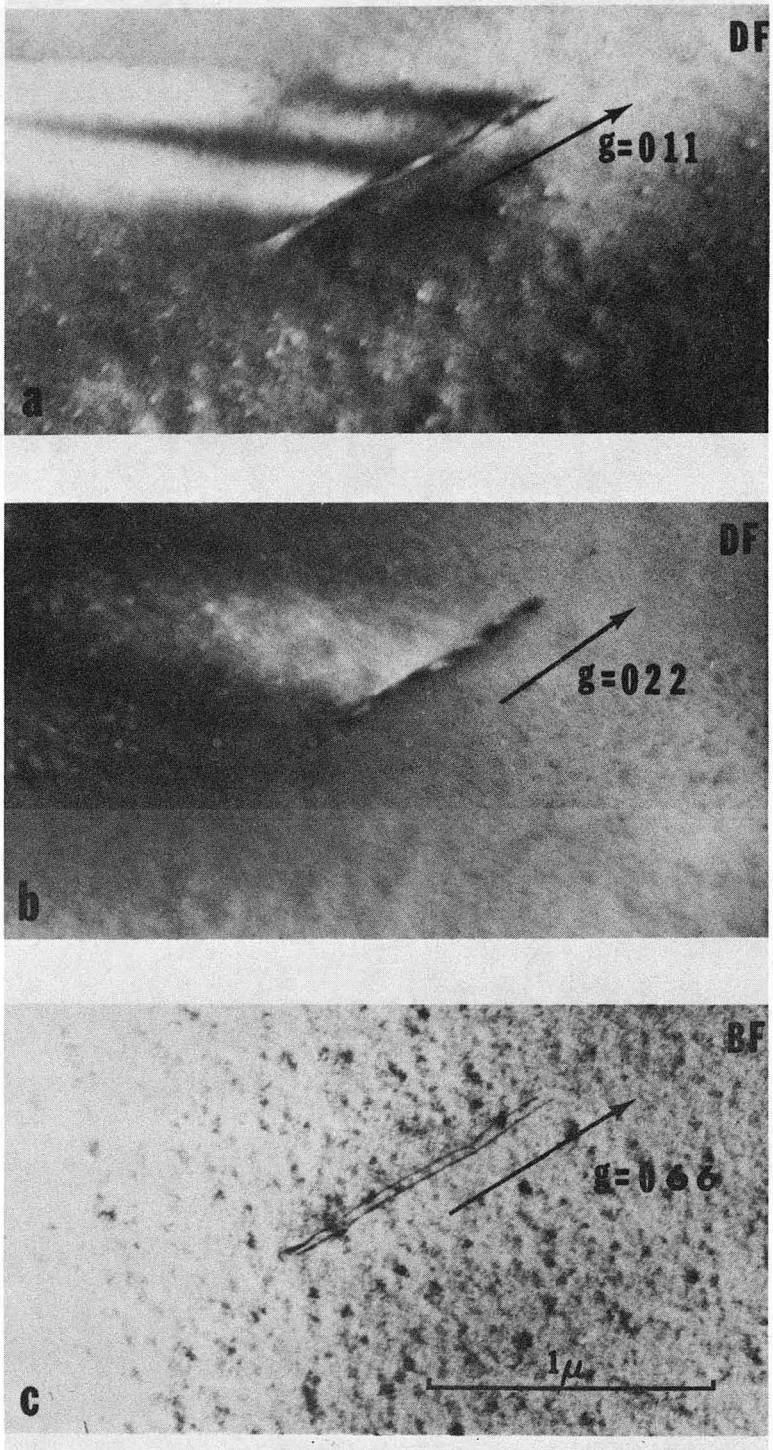


XBB 743-2815

Fig. 18.

LEGAL NOTICE

*This report was prepared as an account of work sponsored by the United States Government. Neither the United States nor the United States Atomic Energy Commission, nor any of their employees, nor any of their contractors, subcontractors, or their employees, makes any warranty, express or implied, or assumes any legal liability or responsibility for the accuracy, completeness or usefulness of any information, apparatus, product or process disclosed, or represents that its use would not infringe privately owned rights.*

*TECHNICAL INFORMATION DIVISION*
*LAWRENCE BERKELEY LABORATORY*
*UNIVERSITY OF CALIFORNIA*
*BERKELEY, CALIFORNIA 94720*